Soft-core baryon-baryon one-boson-exchange models. II. Hyperon-nucleon potential

P. M. M. Maessen, Th. A. Rijken, and J. J. de Swart
University of Nijmegen, Institute for Theoretical Physics, Toernooiveld 1, 6525 ED Nijmegen, The Netherlands
(Received 3 April 1989)

The results of the Nijmegen soft-core potential model are presented for the low-energy *YN* interactions. The *YN* version of the model is obtained by a straightforward extension of the *NN* model through the application of SU(3). The potentials are due to the dominant parts of the π, η, η', ρ, ω, ϕ, δ, ε, and S^* Regge trajectories. This gives the traditional one-boson-exchange potentials. In addition to these, the $J=0$ contributions from the tensor f,f', A_2 and Pomeron trajectories are included in the potentials. The latter give potentials of the Gaussian type. Also the form factors from Regge poles are Gaussian, which guarantees that the potentials have a soft behavior near the origin. The multichannel Schrödinger equation is solved in configuration space for the (partially) nonlocal potentials. We work on the particle basis and include the Coulomb interaction exactly. The meson-baryon coupling constants are calculated via SU(3), using the coupling constants of the *NN* analysis as input. Charge symmetry breaking in the Λp and Λn channels is included. An excellent description is achieved of the available low-energy data per degree of freedom ($\chi^2 \approx 0.58$ for 35 *YN* data). In particular, we were able to fit the inelastic capture ratio at rest perfectly. We have $r_R = 0.471$, where experimentally the average value is $r_R = 0.468 \pm 0.010$. The obtained values for the adjustable mixing angles and $F/(F+D)$ ratios agree very well with the literature. We find $\alpha_{PV} = 0.355$ and $\alpha_V^m = 0.275$. For the scalar-meson mixing angle we obtain $\theta_s = 40.895°$, which lies between the ideal mixing angles for the scalar $q^2\bar{q}^2$ and $q\bar{q}$ states. In the Λp system we find a cusp at the $\Sigma^+ n$ threshold, but there is on the second Riemann sheet no pole in the vicinity causing this cusp. The predictions of the total cross sections up to the pion production threshold are given and compared to the experimental data.

I. INTRODUCTION

For nucleon-nucleon *NN* scattering we have shown [Ref. 1, henceforth referred to as (I)] that a soft-core one-boson-exchange (OBE) model, based on Regge-pole theory, gives an excellent description of the wealthy and precise *NN* data. In (I) only 13 free parameters were used. Moreover, most of these parameters are coupling constants, mixing angles, or $F/(F+D)$ ratios and hence rather physical parameters, for which the fitted values can be checked against those found in other reactions. The nucleon-nucleon soft-core model of (I) can be fully derived in the context of the analytical S-matrix theory.[2] In this framework the consequences of the Regge poles for low energy scattering and the corresponding (relativistic) Lippmann-Schwinger equations can be worked out in a consistent manner. The derivation of the Lippmann-Schwinger equation in this approach has been carried out recently in full detail also for the unequal mass case.[3] This is useful in extending the model to baryon-baryon scattering. In this paper we describe the model for hyperon-nucleon *YN* scattering and discuss the results. Because of the composite nature of the mesons in QCD, the proper description of the OBE potentials is in principle in terms of Regge trajectories. The large N expansion in QCD strongly supports this viewpoint.[4] This is also the case in the Bethe-Salpeter approach to the $Q\bar{Q}$ system, where any reasonable interaction leads to Regge poles. Therefore, in (I) and in this paper the OBE potentials are treated as the dominant parts of the meson Regge trajectories. This also includes the $J=0$ contributions from the tensor trajectories (f, f', and A_2). In elastic scattering, however, the most important exchange at higher energies is pomeron exchange. Therefore in (I) the traditional OBE model was extended by including the Pomeron. An excellent agreement was found between the Pomeron parameters determined from the high-energy and the low-energy *NN* data.

The reasons for a combined study of the *NN* and *YN* interactions are the same as that for our former hard-core model description of the *NN* and *YN* data:[5-7]

(i) To test the assumption of SU(3) symmetry. For example, we want to investigate the properties of the scalar mesons [$\varepsilon(760)$, $S^*(975)$, $\delta(980)$, and $\kappa(1000)$]. Furthermore we want to check whether in a combined *NN* and *YN* analysis the contribution to the interaction from the $J=0$ components of the pomeron, f, f', and A_2 can be included.

(ii) The determination of the $F/(F+D)$ ratios.

(iii) To extract, in spite of the scarce experimental *YN* data, information about scattering lengths, effective ranges, the existence of resonances, etc.

This program appears to be feasible, because a good theoretical description of the *YN* interactions can indeed by given by using SU(3) and the meson-nucleon coupling constants from the *NN* analysis

The interactions in the model are described in terms of the following exchanges.

(1) the pseudoscalar-meson nonet π,η,η',K with the

$\eta-\eta'$ mixing angle $\theta_P=-23.0°$ from the Gell-Mann-Okubo mass formula.

(2) The vector-meson nonet ρ,ϕ,K^*,ω with the $\phi-\omega$ ideal mixing angle $\theta_V=37.56°$.

(3) The scalar-meson nonet $\delta,S^*,\kappa,\varepsilon$ with a free $S^*-\varepsilon$ mixing angle θ_S to be determined in a fit to the *YN* data.

(4) The "diffractive" contribution from the Pomeron P, f, f', and A_2. These interactions will give repulsive contributions to the potentials in all channels of a Gaussian type and can perhaps partly justify the use of hard-cores in our earlier work.

The baryon-baryon-meson vertices are described by coupling constants and form factors, which correspond to the Regge residues. The form factors are taken to be of the Gaussian type, like the residue functions in many Regge-pole models for high-energy scattering. Note also that in nonrelativistic quark models a Gaussian behavior of the form factors is most natural. These form factors evidently guarantee a soft behavior of the potentials in configuration space at small distances.

The physical nature of Pomeron exchange can be understood in the framework of QCD as a two-gluon- (or multigluon-) exchange effect. Low and Nussinov[8] have shown that at high energies Pomeron-exchange and two-gluon-exchange are equivalent. In Ref. 9 it has been demonstrated that this particular QCD picture of the Pomeron leads to a good description of the various diffraction processes. By extrapolating from the higher energies to low energies, using a Regge-pole model, the (multi-) gluon-exchange potential between two baryons was found in Ref. 2. In *NN* interactions the inclusion of the Pomeron improved in particular the electric ω coupling considerably.[1] The role of the Pomeron for low-energy πN and KN scattering has been demonstrated convincingly using finite-energy sum rules (FESR).[10] In fact, it has been shown that the background amplitude, which remains after the subtraction of the known resonances, produces the Pomeron contribution at high energies via FESR.[11]

In this work we check whether a strong repulsion from the Pomeron and the tensor mesons together with Gaussian form factors can also give a high quality description of the *YN* data. By high quality we understand here a *YN* fit with low χ^2 and such that, while keeping the constraints forced on the potentials by the *NN* fit, the free parameters with a clear physical significance, like, e.g., the $F/(F+D)$ ratios α_{PV} and α_V^m, assume realistic values.

In this paper we treat in detail the following *YN* reactions: (i) the coupled channels $\Lambda p\to\Lambda p,\Sigma^+n,\Sigma^0p$; (ii) the coupled channels $\Sigma^-p\to\Sigma^-p,\Sigma^0n,\Lambda n$; and (iii) the single channel $\Sigma^+p\to\Sigma^+p$. It turns out that starting from the soft-core OBE model of Ref. 1, we are indeed able to achieve a very good description of the *YN* data and at the same time maintain values for the free parameters which are very consistent with other findings. As an application of the obtained potentials, the properties of the hyperfragments might be predicted. The determined value for the $F/(F+D)$ ratio α_{PV} for the pseudoscalar mesons is the same as that found in the weak interactions.[12,13] Also the value obtained for the magnetic ratio of the vector mesons is in perfect agreement with nonstatic SU(6).[14]

Like in previous work of the Nijmegan group on *YN* (e.g., Refs. 6 and 7), we use SU(3) symmetry for the coupling constants. SU(3) breaking is introduced by using the physical masses of the mesons and baryons in the potentials and Schrödinger equation (see Refs. 6, 7, and 15); allowing for meson mixing within a nonet ($\eta-\eta'$, $\omega-\phi$, $\varepsilon-S^*$); including charge symmetry breaking (CSB) (Ref. 16) due to $\Lambda\Sigma$ mixing, which, for example, introduces a one-pion-exchange potential in the ΛN channel; and taking into account the Coulomb interaction. In order to include the Coulomb interaction exactly, and to account as much as possible for the mass differences between the baryons, we solve the multichannel Schrödinger equation on the physical particle basis. However, the nuclear potentials are calculated on the isospin basis, in order to limit the number of different form factors (see Sec. VII).

In *NN* interactions we have fitted all partial waves with only one form factor parameter. For *YN* it appears to be impossible to use only one form factor for all channels. This would either introduce unobserved bound states in the model or make a fit to the *YN* data impossible. Therefore we have to use several. (Note, however, that for avoiding unobserved bound states, the freedom to adjust form factors is much less powerful than the freedom of changing hard cores. For instance, changing the form factors does not change the volume integral of the potentials). In our approach, we have introduced the form factors *per channel*. For several reasons we did not choose to differentiate between the different kind of mesons with respect to the form factor. First, that would introduce more parameters in the model for both *NN* and *YN*. Secondly, it is believed that the nature of the short-range potentials is at present, at least quantitatively, poorly understood. Probably any OBE model also effectively includes forces which are not of the OBE type. It is clearly allowable to parametrize these unknown short-range forces for the different *YN* channels independently.

The contents of this paper are as follows. In Sec. II we define the OBE potentials for the Lippmann-Schwinger equation. In Sec. III the OBE potentials in momentum space for pseudoscalar, vector, scalar, and diffractive exchanges are given and discussed. In Sec. IV we systematically describe the Fourier transformation to configuration space for the potentials of Sec. III. In Sec. V we outline the treatment of the multichannel Schrödinger equation with the nonlocal central potentials derived in Sec. III. In Sec. VI we discuss the form factor assignments in the context of SU(3). In Sec. VII the results for the coupling constants, $F/(F+D)$ ratios, and mixing angles are discussed and compared with the literature and the nonrelativistic quark model. In Sec. VIII we present the results of the fit to the *YN* data. Here the results for the Λp, Σ^-p, and Σ^+p data are shown and discussed in detail. At several points in Secs. VII and VIII the results are compared with the former hard-core models for *YN* scattering of the Nijmegen group (Refs. 6 and 7).

II. DEFINITION OF THE POTENTIALS FOR THE LIPPMANN-SCHWINGER EQUATION

We consider the hyperon-nucleon reactions

$$Y(p_1,s_1)+N(p_2,s_2)\to Y'(p_1',s_1')+N'(p_2',s_2')\ . \qquad (1)$$

As in Ref. 6, whose conventions we will follow in this paper, we will also refer to Y and Y' as particles 1 and 3 and to N and N' as particles 2 and 4. The four momentum of particle i is $p_i=(E_i,\mathbf{p}_i)$, where $E_i=(\mathbf{p}_i^2+M_i^2)^{1/2}$ and M_i is the mass. The transition amplitude matrix M is related to the S matrix via

$$\langle f|S|i\rangle=\langle f|i\rangle-i(2\pi)^4\delta^4(P_f-P_i)\langle f|M|i\rangle\ , \tag{2}$$

where $P_i=p_1+p_2$ and $P_f=p_1'+p_2'$ represent the total four momentum for the initial state $|i\rangle$ and the final state $|f\rangle$. The latter refer to the two-particle states, which we normalize in the following way:

$$\langle \mathbf{p}_1',\mathbf{p}_2'|\mathbf{p}_1,\mathbf{p}_2\rangle=(2\pi)^3 2E(\mathbf{p}_1)\delta^3(\mathbf{p}_1'-\mathbf{p}_1)\cdot(2\pi)^3 2E(\mathbf{p}_2)\delta^3(\mathbf{p}_2'-\mathbf{p}_2)\ . \tag{3}$$

Three-dimensional integral equations for the amplitudes $\langle f|M|i\rangle$ can be derived in various ways. See, for example, Refs. 6, 17, 18, 19, and 20. In Ref. 3 is given a derivation based on two-particle unitarity and the analyticity properties of the amplitudes, using the N/D formalism. The equation obtained with this method is

$$M_{fi}(\mathbf{q}_f,\mathbf{q}_i;s)=W_{fi}(\mathbf{q}_f,\mathbf{q}_i;s)+\frac{1}{(2\pi)^3}\sum_n\int d^3k_n\,W_{fn}(\mathbf{q}_f,\mathbf{k}_n;s)G_0(\mathbf{k}_n,s)M_{ni}(\mathbf{k}_n,\mathbf{q}_i;s)\ , \tag{4}$$

where $\mathbf{q}_i$ and $\mathbf{q}_f$ denote the initial- and final-state momenta, and

$$G_0(\mathbf{k};s)=\frac{1}{2}\frac{E_1(\mathbf{k})+E_2(\mathbf{k})}{E_1(\mathbf{k})E_2(\mathbf{k})}\times\{s-[E_1(\mathbf{k})+E_2(\mathbf{k})]^2+i\varepsilon\}^{-1}\ , \tag{5}$$

with $s=[E_1(\mathbf{p})+E_2(\mathbf{p})]^2$. This follows from Eq. (4.27) in Ref. 3. This same equation has been derived by Gersten, Verhoeven, and de Swart[17] in the context of an approach which uses the Bethe-Salpeter equation. Also in Ref. 3 it is shown that for pseudopotential $\langle f|W|i\rangle$ corresponds in the pole approximation to the Feynman-amplitudes for OBE exchanges with form factors at the baryon-baryon-meson (BBM) vertices. In order to arrive at a Lippmann-Schwinger equation, we choose a new Green's function $g(\mathbf{k};s)$ which satisfies a dispersion relation in $\mathbf{p}^2(s)$ rather than in s. Then we get, like in Refs. 3, 6, and 20,

$$g(\mathbf{k}_n;s)=\frac{-1}{2[E_1(\mathbf{k}_n)+E_2(\mathbf{k}_n)]}(\mathbf{k}_n^2-\mathbf{q}_n^2-i\varepsilon)^{-1}\ , \tag{6}$$

where $\mathbf{q}_n$ is the on-energy-shell momentum. This Green's function is eventually used in the integral equation (4) instead of $G_0(\mathbf{k}_n;s)$. So the corrections to $\langle f|W|i\rangle$ due to the transformation of the Green's functions are neglected. They are of higher order in the couplings and are usually discarded in an OBE approach. With the substitution of g for G, Eq. (5) becomes identical to Eq. (2.19) of Ref. 6. From now on we follow Sec. II of Ref. 6 in detail. The transformation to the nonrelativistic normalization of the two-particle states leads to states with

$$(\mathbf{p}_1',s_1';\mathbf{p}_2',s_2'|\mathbf{p}_1,s_1;\mathbf{p}_2,s_2)=(2\pi)^6\delta^3(\mathbf{p}_1'-\mathbf{p}_1)\delta^3(\mathbf{p}_2'-\mathbf{p}_2)\delta_{s_1',s_1}\delta_{s_2',s_1}\ . \tag{7}$$

For these states we define the T matrix by

$$(f|T|i)=[4M_{34}(E_3+E_4)]^{-1/2}\langle f|M|i\rangle\times[4M_{12}(E_1+E_2)]^{-1/2}\ , \tag{8}$$

and get from Eq. (4) the Lippmann-Schwinger equation

$$(3,4|T|1,2)=(3,4|V|1,2)+\frac{1}{(2\pi)^3}\sum_n\int d^3k_n(3,4|V|n_1,n_2)\frac{2M_{n_1,n_2}}{\mathbf{q}_n^2-\mathbf{k}_n^2+i\varepsilon}(n_1,n_2|T|1,2)\ , \tag{9}$$

and where analogously to Eq. (8) the potential V is defined as

$$(f|V|i)=[4M_{34}(E_3+E_4)]^{-1/2}\langle f|W|i\rangle\times[4M_{12}(E_1+E_2)]^{-1/2}\ . \tag{10}$$

Using rotational invariance and parity conservation we expand the T matrix, which is a 4×4 matrix in Pauli-spinor space, into a complete set of Pauli-spinor invariants[6,15]

$$T=\sum_{i=1}^{8}T_i(\mathbf{q}_f^2,\mathbf{q}_i^2,\mathbf{q}_i\cdot\mathbf{q}_f)P_i\ . \tag{11}$$

Introducing

$$\mathbf{q}=\tfrac{1}{2}(\mathbf{q}_f+\mathbf{q}_i),\quad \mathbf{k}=\mathbf{q}_f-\mathbf{q}_i\ ,\qquad \mathbf{n}=\mathbf{q}_i\times\mathbf{q}_f=\mathbf{q}\times\mathbf{k}\ , \tag{12}$$

we choose for the operators P_i in spin space

$$\begin{aligned}&P_1=1\ ,\\ &P_2=\boldsymbol{\sigma}_1\cdot\boldsymbol{\sigma}_2\ ,\\ &P_3=(\boldsymbol{\sigma}_1\cdot\mathbf{k})(\boldsymbol{\sigma}_2\cdot\mathbf{k})-\tfrac{1}{3}(\boldsymbol{\sigma}_1\cdot\boldsymbol{\sigma}_2)\mathbf{k}^2\ ,\\ &P_4=\frac{i}{2}(\boldsymbol{\sigma}_1+\boldsymbol{\sigma}_2)\cdot\mathbf{n}\ ,\\ &P_5=(\boldsymbol{\sigma}_1\cdot\mathbf{n})(\boldsymbol{\sigma}_2\cdot\mathbf{n})\ ,\end{aligned} \tag{13}$$

$$P_6=\frac{i}{2}(\sigma_1-\sigma_2)\cdot\mathbf{n}\ ,$$

$$P_7=(\sigma_1\cdot\mathbf{q})(\sigma_2\cdot\mathbf{k})+(\sigma_1\cdot\mathbf{k})(\sigma_2\cdot\mathbf{q})\ ,$$

$$P_8=(\sigma_1\cdot\mathbf{q})(\sigma_2\cdot\mathbf{k})-(\sigma_1\cdot\mathbf{k})(\sigma_2\cdot\mathbf{q})\ .$$

Here we follow Refs. 6 and 15, except that here we have chosen P_3 to be a purely "tensor-force" operator.

In the OBEP approximation we consider only second-order irreducible diagrams contributing to the kernel, i.e., $W=M^{\mathrm{irr}(2)}$. Similarly to Eq. (11) we expand the potentials V. Again following Ref. 6, we neglect the potential forms P_7 and P_8, and also the dependence of the potentials on $\mathbf{k}\cdot\mathbf{q}$. Consequently the potentials can be expanded as follows:

$$V=\sum_{i=1}^{6}V_i(\mathbf{k}^2,\mathbf{q}^2)P_i\ . \tag{14}$$

In the following we will exploit this decomposition extensively.

III. ONE-BOSON-EXCHANGE POTENTIALS IN MOMENTUM SPACE

In this section we extend the NN potentials given in Ref. 1 to the YN channels. The local interaction Hamilton densities for the different couplings are (a) pseudoscalar-meson exchange

$$\mathcal{H}_{\mathrm{PV}}=i\frac{f_P}{m_{\pi^+}}\bar{\psi}\gamma_\mu\gamma_5\psi\partial^\mu\phi_P\ , \tag{15}$$

(b) vector-meson exchange

$$\mathcal{H}_V=ig_V\bar{\psi}\gamma_\mu\psi\phi_V^\mu+\frac{f_V}{4\mathcal{M}}\bar{\psi}\sigma_{\mu\nu}\psi(\partial^\mu\phi_V^\nu-\partial^\nu\phi_V^\mu)\ , \tag{16}$$

and (c) scalar-meson exchange

$$\mathcal{H}_S=g_S\bar{\psi}\psi\phi_S\ , \tag{17}$$

where $\sigma_{\mu\nu}=[\gamma_\mu,\gamma_\nu]/2i$ and m_{π^+} and $\mathcal{M}$ are scaling masses, chosen to be the charged pion and the proton mass, respectively. Note that the vertices for "diffractive" exchange have the same Lorentz structure as those for scalar-meson-exchange.

Including form factors $f(\mathbf{x}'-\mathbf{x})$, the interaction densities are modified to

$$H_X(\mathbf{x})=\int d^3x'f(\mathbf{x}'-\mathbf{x})\mathcal{H}_X(\mathbf{x}')\ , \tag{18}$$

where $X=\mathrm{PV}$, V, or S. Because of this "convolutive" form, the potentials in momentum space are the same as for point interactions, except that the coupling constants are multiplied by the Fourier transform of the form factors.

In the derivation of V_i we use the following approximations, which can be justified for low-energy scattering.

(1) We make the expansion

$$E(p)\approx(\mathbf{k}^2/4+\mathbf{q}^2+M^2)^{1/2}\approx M+\mathbf{k}^2/8M+\mathbf{q}^2/2M$$

and keep only terms up to first order in $\mathbf{k}^2/M$ and $\mathbf{q}^2/M$, except for the form factors where the full $\mathbf{k}^2$ dependence is kept throughout the calculations. Notice that the Gaussian form factors suppress the high $\mathbf{k}^2$ contributions strongly.

(2) In the meson propagators,

$$(p_1-p_3)^2+m^2\approx(\mathbf{k}^2+m^2)\ .$$

(3) When two different hyperons are involved at a BBM vertex (e.g., Λ and Σ) their average mass is used in the potentials and the nonzero component of the momentum transfer is accounted for by using an effective mass in the meson propagator (for details see Refs. 21 and 15).

Due to the approximations we get only a linear dependence on $\mathbf{q}^2$ for V_1. In the following, we write

$$V_1(\mathbf{k}^2,\mathbf{q}^2)=V_{1a}(\mathbf{k}^2)+V_{1b}(\mathbf{k}^2)\mathbf{q}^2\ . \tag{19}$$

The OBE potentials are now obtained in the standard way (see, e.g., Refs. 1 and 6) by evaluating the YN interaction by Born approximation. We write the potentials V_i of Eqs. (14) and (19) in the form

$$V_i(\mathbf{k}^2,\mathbf{q}^2)=\sum_X\Omega_i^{(X)}(\mathbf{k}^2)\cdot\Delta^{(X)}(\mathbf{k}^2,m^2,\Lambda^2)\ , \tag{20}$$

where $X=P$, V, S, and D ($P=$pseudoscalar, $V=$vector, $S=$scalar, and $D=$diffractive). Furthermore

$$\Delta^{(X)}(\mathbf{k}^2,m^2,\Lambda^2)=\frac{1}{\mathbf{k}^2+m^2}\cdot e^{-\mathbf{k}^2/\Lambda^2} \tag{21}$$

for $X=P,V,S$, and

$$\Delta^{(D)}(\mathbf{k}^2,m^2,\Lambda^2)=\frac{1}{\mathcal{M}^2}e^{-\mathbf{k}^2/(4m_p^2)} \tag{22}$$

for $X=D$. In the latter expression $\mathcal{M}$ is a universal scaling mass, which is again taken to be the proton mass. The mass parameter m_p controls the $\mathbf{k}^2$ dependence of the Pomeron, f, f', A_2, and K^{**} potentials. For the nonstrange mesons we find, using the approximations (1)–(5), the following contributions to the different $\Omega_i^{(X)}$.

(a) Pseudoscalar-meson exchange:

$$\Omega_2^{(P)}=g_{13}^Pg_{24}^P\left[\frac{\mathbf{k}^2}{12M_YM_N}\right]\ ,$$
$$\Omega_3^{(P)}=-g_{13}^Pg_{24}^P\left[\frac{1}{4M_YM_N}\right]\ . \tag{23}$$

(b) Vector-meson exchange:

$$\Omega_{1a}^{(V)}=\left[g_{13}^{V}g_{24}^{V}\left[1-\frac{\mathbf{k}^2}{8M_YM_N}\right]-g_{13}^{V}f_{24}^{V}\frac{\mathbf{k}^2}{4\mathcal{M}M_N}\right.$$
$$\left.-f_{13}^{V}g_{24}^{V}\frac{\mathbf{k}^2}{4\mathcal{M}M_Y}+f_{13}^{V}f_{24}^{V}\frac{\mathbf{k}^4}{16\mathcal{M}^2M_YM_N}\right],$$
$$\Omega_{1b}^{(V)}=g_{13}^{V}g_{24}^{V}\left[\frac{3}{2M_YM_N}\right],$$
$$\Omega_{2}^{(V)}=-\tfrac{2}{3}\mathbf{k}^2\Omega_{3}^{(V)},$$
$$\Omega_{3}^{(V)}=\left[\left[g_{13}^{V}+f_{13}^{V}\frac{M_Y}{\mathcal{M}}\right]\left[g_{24}^{V}+f_{24}^{V}\frac{M_N}{\mathcal{M}}\right]\right.$$
$$\left.-f_{13}^{V}f_{24}^{V}\frac{\mathbf{k}^2}{8\mathcal{M}^2}\right]\Big/(4M_YM_N),\qquad(24)$$
$$\Omega_{4}^{(V)}=-\left[12g_{13}^{V}g_{24}^{V}+8(g_{13}^{V}f_{24}^{V}+f_{13}^{V}g_{24}^{V})\frac{\sqrt{M_YM_N}}{\mathcal{M}}\right.$$
$$\left.-f_{13}^{V}f_{24}^{V}\frac{3\mathbf{k}^2}{\mathcal{M}^2}\right]\Big/(8M_YM_N),$$
$$\Omega_{5}^{(V)}=-\left[g_{13}^{V}g_{24}^{V}+4(g_{13}^{V}f_{24}^{V}+f_{13}^{V}g_{24}^{V})\frac{\sqrt{M_YM_N}}{\mathcal{M}}\right.$$
$$\left.+8f_{13}^{V}f_{24}^{V}\frac{M_YM_N}{\mathcal{M}^2}\right]\Big/(16M_Y^2M_N^2),$$
$$\Omega_{6}^{(V)}=-\left[\left[g_{13}^{V}g_{24}^{V}+f_{13}^{V}f_{24}^{V}\frac{\mathbf{k}^2}{4\mathcal{M}^2}\right]\frac{(M_N^2-M_Y^2)}{4M_Y^2M_N^2}\right.$$
$$\left.-(g_{13}^{V}f_{24}^{V}-f_{13}^{V}g_{24}^{V})\frac{1}{(\mathcal{M}^2M_YM_N)^{1/2}}\right].$$

(c) Scalar-meson exchange:

$$\Omega_{1a}^{(S)}=-g_{13}^{S}g_{24}^{S}\left[1+\frac{\mathbf{k}^2}{8M_YM_N}\right],$$
$$\Omega_{1b}^{(S)}=g_{13}^{S}g_{24}^{S}\frac{1}{2M_YM_N},$$
$$\Omega_{4}^{(S)}=-g_{13}^{S}g_{24}^{S}\frac{1}{2M_YM_N},\qquad(25)$$
$$\Omega_{5}^{(S)}=g_{13}^{S}g_{24}^{S}\frac{1}{16M_Y^2M_N^2},$$
$$\Omega_{6}^{(S)}=-g_{13}^{S}g_{24}^{S}\frac{(M_N^2-M_Y^2)}{4M_YM_N}.$$

(d) "diffractive-exchange" (Pomeron, f,f',A_2): The Ω_i^D are the same as for scalar-meson-exchange Eq. (25), but with $\pm g_{13}^{S}g_{24}^{S}$ replaced by $\mp g_{13}^{D}g_{24}^{D}$.

In the expressions for Ω^P, Ω^V, and Ω^S given previously, M_Y and M_N denote the mean hyperon and nucleon mass, respectively; $M_Y=(M_1+M_3)/2$ and $M_N=(M_2+M_4)/2$; and m denotes the mass of the exchanged meson. The form factor mass Λ will be discussed in Sec. VI. In deriving these formulas for the Ω's we used $1/M_N^2+1/M_Y^2\approx 2/M_NM_Y$, which holds to a good approximation since the mass differences between the baryons are not large.

For the strangeness carrying exchanges (K,K^*,κ,K^{**}) we have a complete symmetric appearance of M_Y and M_N and an additional minus sign. (For the details see Ref. 6.) Therefore the resulting potentials can be obtained from those given in Eqs. (23)–(25), by replacing both M_Y and M_N by $(M_YM_N)^{1/2}$ and adding a minus sign. Furthermore we get non-negligible contributions from the second part of the vector-meson propagator $(k_\mu k_\nu/m^2)$ of the K^* meson giving

$$-V_i^{K^*}=V_i^{(V)}-\frac{(M_3-M_1)(M_4-M_2)}{m^2}V_i^{(S)},\qquad(26)$$

where in $V_i^{(S)}$ the vector-meson-coupling constants have to be used, and M_Y and M_N have to be replaced by $(M_YM_N)^{1/2}$.

IV. ONE-BOSON-EXCHANGE POTENTIALS IN CONFIGURATION SPACE

In configuration space we describe the YN interactions by potentials of the general form

$$V=\{V_C(r)+V_\sigma(r)\boldsymbol{\sigma}_1\cdot\boldsymbol{\sigma}_2+V_T(r)S_{12}+V_{\rm SO}(r)\mathbf{L}\cdot\mathbf{S}$$
$$+V_Q(r)Q_{12}+V_{\rm ASO}(r)\tfrac{1}{2}(\boldsymbol{\sigma}_1-\boldsymbol{\sigma}_2)\cdot\mathbf{L}$$
$$-\tfrac{1}{2}[\nabla^2\phi(r)+\phi(r)\nabla^2]\}\cdot P,\qquad(27)$$

where

$$S_{12}=3\frac{(\boldsymbol{\sigma}_1\cdot\mathbf{r})(\boldsymbol{\sigma}_2\cdot\mathbf{r})}{r^2}-(\boldsymbol{\sigma}_1\cdot\boldsymbol{\sigma}_2),\qquad(28)$$

$$Q_{12}=\tfrac{1}{2}[(\boldsymbol{\sigma}_1\cdot\mathbf{L})(\boldsymbol{\sigma}_2\cdot\mathbf{L})+(\boldsymbol{\sigma}_2\cdot\mathbf{L})(\boldsymbol{\sigma}_1\cdot\mathbf{L})].\qquad(29)$$

The exchange operator $P=1$ for hypercharge $Y=0$ exchange and $P=-P_xP_\sigma$ for $Y\neq 0$ exchange (K,K^*,κ,K^{**}), where P_x and P_σ are the space and spin exchange operators (for a discussion see Ref. 6). The Fourier transformation of the nonlocal operators having a linear $\mathbf{q}^2$ dependence is given in Ref. 1, Eqs. (10) and (11).

The potentials in Eq. (27) are related to those in Eqs. (20)–(25), by the Fourier-Bessel transforms

$$V_C(r)=(1/2\pi^2)\int dk\,k^2j_0(kr)[V_{1a}(k^2)-\tfrac{1}{4}k^2V_{1b}(k^2)],$$
$$V_\sigma(r)=(1/2\pi^2)\int dk\,k^2j_0(kr)V_2(k^2),$$
$$V_T(r)=-(1/6\pi^2)\int dk\,k^4j_2(kr)V_3(k^2),$$
$$V_{\rm SO}(r)=(1/2\pi^2r)\int dk\,k^3j_1(kr)V_4(k^2),\qquad(30)$$
$$V_Q(r)=-(1/2\pi^2r^2)\int dk\,k^4j_2(kr)V_5(k^2),$$
$$V_{\rm ASO}(r)=(1/2\pi^2r)\int dk\,k^3j_1(kr)V_6(k^2),$$
$$\phi(r)=(1/2\pi^2)\int dk\,k^2j_0(kr)V_{1b}(k^2),$$

where k runs from 0 to ∞ and the j_l are the spherical Bessel functions of the first kind.[22] In this form the relation between the potentials in momentum and config-

uration space is explicit and the behavior of the potentials at $r=0$ is clearly exhibited. Due to the Gaussian form factors the k integrals exist for all r.

With the momentum space potentials of Sec. III, these Fourier transforms can be carried out analytically.[1] For this we use the ϕ functions of Ref. 1, Eqs. (12), etc., which are defined in terms of the integrals (30) by taking

$$V_i=\exp(-k^2/\Lambda^2)/(k^2+m^2)=\Delta(k^2,m^2,\Lambda^2)$$

which gives

$$\begin{aligned}
&\frac{m}{4\pi}(-m^2)^n\phi_C^n(r)=(1/2\pi^2)\int dk\, k^2 j_0(kr)(k^2)^n\Delta(k^2,m^2,\Lambda^2)\ ,\\
&-\frac{m^3}{4\pi}(-m^2)^n\phi_T^n(r)=-(1/6\pi^2)\int dk\, k^4 j_2(kr)(k^2)^n\Delta(k^2,m^2,\Lambda^2)\ ,\\
&\frac{m^3}{4\pi}(-m^2)^n\phi_{\rm SO}^n(r)=(1/2\pi^2 r)\int dk\, k^3 j_1(kr)(k^2)^n\Delta(k^2,m^2,\Lambda^2)\ .
\end{aligned}\tag{31}$$

Introducing the auxiliary functions $\Delta_X^n(\Lambda,r)$ by

$$\begin{aligned}
&\frac{m}{4\pi}(-m^2)^{n+1}\Delta_C^{n+1}(\Lambda,r)=(1/2\pi^2)\int dk\, k^2 j_0(kr)(k^2)^n\exp(-k^2/\Lambda^2)\ ,\\
&-\frac{m^3}{4\pi}(-m^2)^{n+1}\Delta_T^{n+1}(\Lambda,r)=-(1/6\pi^2)\int dk\, k^4 j_2(kr)(k^2)^n\exp(-k^2/\Lambda^2)\ ,\\
&\frac{m^3}{4\pi}(-m^2)^{n+1}\Delta_{\rm SO}^{n+1}(\Lambda,r)=(1/2\pi^2 r)\int dk\, k^3 j_1(kr)(k^2)^n\exp(-k^2/\Lambda^2)\ ,
\end{aligned}\tag{32}$$

one can readily show, by making the substitution $k^2\to(k^2+m^2)-m^2$, that

$$\phi_X^{n+1}(r)=\phi_X^n(r)+\Delta_X^{n+1}(\Lambda,r)\tag{33}$$

for $X=C$, T, and SO. Also one has

$$\Delta_X^{n+1}(\Lambda,r)=-\frac{1}{2}\left[\frac{\Lambda}{m}\right]^2\left[\Lambda\frac{d}{d\Lambda}\right]\Delta_X^n(\Lambda,r)\ .\tag{34}$$

The functions $\phi_C^0(r)$, $\phi_T^0(r)$, and $\phi_{\rm SO}^0(r)$ are given in Ref. 1, Eqs. (13), (17), and (20). They read

$$\begin{aligned}
\phi_C^0(r)&=\exp(m^2/\Lambda^2)\left[e^{-mr}\mathrm{erfc}\left[-\frac{\Lambda r}{2}+\frac{m}{\Lambda}\right]-e^{mr}\mathrm{erfc}\left[\frac{\Lambda r}{2}+\frac{m}{\Lambda}\right]\right]\Big/2mr\ ,\\
\phi_T^0(r)&=\left\{\exp(m^2/\Lambda^2)\left[[1+mr+\tfrac{1}{3}(mr)^2]e^{-mr}\mathrm{erfc}\left[-\frac{\Lambda r}{2}+\frac{m}{\Lambda}\right]-[1-mr+\tfrac{1}{3}(mr)^2]e^{mr}\mathrm{erfc}\left[\frac{\Lambda r}{2}+\frac{m}{\Lambda}\right]\right]\right.\\
&\quad\left.-\frac{4}{\sqrt{\pi}}\left[\frac{\Lambda r}{2}\right]\left[1+\frac{2}{3}\left[\frac{\Lambda r}{2}\right]^2\right]\exp\left[-\left[\frac{\Lambda r}{2}\right]^2\right]\right\}\Big/2(mr)^3\ ,\\
\phi_{\rm SO}^0(r)&=\left\{\exp(m^2/\Lambda^2)\left[(1+mr)e^{-mr}\mathrm{erfc}\left[-\frac{\Lambda r}{2}+\frac{m}{\Lambda}\right]-(1-mr)e^{mr}\mathrm{erfc}\left[\frac{\Lambda r}{2}+\frac{m}{\Lambda}\right]\right]\right.\\
&\quad\left.-\frac{4}{\sqrt{\pi}}\left[\frac{\Lambda r}{2}\right]\exp\left[-\left[\frac{\Lambda r}{2}\right]^2\right]\right\}\Big/2(mr)^3\ .
\end{aligned}\tag{35}$$

For $\Delta_C^1(\Lambda,r)$, $\Delta_T^1(\Lambda,r)$, and $\Delta_{\rm SO}^1(\Lambda,r)$ we have [compare Ref. 1, Eqs. (14), (18), and (21)]

$$\begin{aligned}
\Delta_C^1(\Lambda,r)&=-\frac{1}{2\sqrt{\pi}}\left[\frac{\Lambda}{m}\right]^3\exp\left[-\left[\frac{\Lambda r}{2}\right]^2\right]\ ,\\
\Delta_T^1(\Lambda,r)&=-\frac{1}{6\sqrt{\pi}}\left[\frac{\Lambda}{m}\right]^5\exp\left[-\left[\frac{\Lambda r}{2}\right]^2\right]\left[\frac{\Lambda r}{2}\right]^2\ ,\\
\Delta_{\rm SO}^1(\Lambda,r)&=-\frac{1}{4\sqrt{\pi}}\left[\frac{\Lambda}{m}\right]^5\exp\left[-\left[\frac{\Lambda r}{2}\right]^2\right]\ .
\end{aligned}\tag{36}$$

It is clear from Eq. (30) that for $V_\sigma(r)$ and $\phi(r)$ the basic integrals needed for the Fourier transformation are the same as for $V_C(r)$, i.e., $\phi_C^n(r)$. Similarly the basic integrals for $V_{\rm ASO}(r)$ and $V_Q(r)$ are readily given in terms of $\phi_{\rm SO}^n(r)$ and $\phi_T^n(r)$, respectively. For instance, Eq. (22) of Ref. 1 concerning the Fourier transformation of the quadratic spin-orbit potential can readily be obtained from the formulas given in this paper.

For the "diffractive" exchanges, only Gaussian integrals occur in the course of the Fourier transformation and they can be evaluated in terms of the Δ_X^n functions or directly [see Ref. 1, Eqs. (25)–(28)].

Using these Fourier-Bessel transforms one can perform the Fourier transformation in a straightforward manner. The results are the following.

(a) Pseudoscalar-meson exchange:

$$V_{\rm PS}(r)=\frac{m}{4\pi}\left[g_{13}^P g_{24}^P \frac{m^2}{4M_Y M_N}[\tfrac{1}{3}(\boldsymbol{\sigma}_1\cdot\boldsymbol{\sigma}_2)\phi_C^1+S_{12}\phi_T^0]\right]P\ . \tag{37}$$

(b) Vector-meson exchange:

$$\begin{aligned}V_V(r)=\frac{m}{4\pi}\Bigg[&\left\{g_{13}^V g_{24}^V\left[\phi_C^0+\frac{m^2}{2M_Y M_N}\phi_C^1-\frac{3}{4M_Y M_N}(\nabla^2\phi_C^0+\phi_C^0\nabla^2)\right]\right.\\&\left.+\left[g_{13}^V f_{24}^V\frac{m^2}{4\mathcal{M}M_N}+f_{13}^V g_{24}^V\frac{m^2}{4\mathcal{M}M_Y}\right]\phi_C^1+f_{13}^V f_{24}^V\frac{m^4}{16\mathcal{M}^2M_Y}\phi_C^2\right\}\\&+\frac{m^2}{4M_Y M_N}\left\{\left[\left[g_{13}^V+f_{13}^V\frac{M_Y}{\mathcal{M}}\right]+\left[g_{24}^V+f_{24}^V\frac{M_N}{\mathcal{M}}\right]\right]\phi_C^1+f_{13}^V f_{24}^V\frac{m^2}{8\mathcal{M}^2}\phi_C^2\right\}\tfrac{2}{3}(\boldsymbol{\sigma}_1\cdot\boldsymbol{\sigma}_2)\\&-\frac{m^2}{4M_Y M_N}\left\{\left[\left[g_{13}^V+f_{13}^V\frac{M_Y}{\mathcal{M}}\right]+\left[g_{24}^V+f_{24}^V\frac{M_N}{\mathcal{M}}\right]\right]\phi_T^0+f_{13}^V f_{24}^V\frac{m^2}{8\mathcal{M}^2}\phi_T^1\right\}S_{12}\\&-\frac{m^2}{M_Y M_N}\left\{\left[\tfrac{3}{2}g_{13}^V g_{24}^V+\left[g_{13}^V f_{24}^V+f_{13}^V g_{24}^V\right]\frac{\sqrt{M_Y M_N}}{\mathcal{M}}\right]\phi_{\rm SO}^0+\tfrac{3}{8}f_{13}^V f_{24}^V\frac{m^2}{\mathcal{M}^2}\phi_{\rm SO}^1\right\}\mathbf{L}\cdot\mathbf{S}\\&+\frac{m^4}{16M_Y^2M_N^2}\left\{\left[g_{13}^V g_{24}^V+4(g_{13}^V f_{24}^V+f_{13}^V g_{24}^V)\frac{\sqrt{M_Y M_N}}{\mathcal{M}}+8f_{13}^V f_{24}^V\frac{M_Y M_N}{\mathcal{M}^2}\right]\right\}\frac{3}{(mr)^2}\phi_T^0 Q_{12}\\&-\frac{m^2}{M_Y M_N}\left\{\left[\left[g_{13}^V g_{24}^V-f_{13}^V f_{24}^V\frac{m^2}{\mathcal{M}^2}\right]\frac{(M_N^2-M_Y^2)}{4M_Y M_N}\right.\right.\\&\left.\left.-(g_{13}^V f_{24}^V-f_{13}^V g_{24}^V)\frac{\sqrt{M_Y M_N}}{\mathcal{M}}\right]\phi_{\rm SO}^0\right\}\cdot\tfrac{1}{2}(\boldsymbol{\sigma}_1-\boldsymbol{\sigma}_2)\cdot\mathbf{L}\Bigg]P\ .\end{aligned} \tag{38}$$

(c) Scalar-meson exchange:

$$\begin{aligned}V_S(r)=-\frac{m}{4\pi}\Bigg[&g_{13}^S g_{24}^S\left\{\left[\phi_C^0-\frac{m^2}{4M_Y M_N}\phi_C^1\right]+\frac{m^2}{2M_Y M_N}\phi_{\rm SO}^0\mathbf{L}\cdot\mathbf{S}+\frac{m^4}{16M_Y^2M_N^2}\frac{3}{(mr)^2}\phi_T^0 Q_{12}\right.\\&\left.+\frac{m^2}{M_Y M_N}\left[\frac{(M_N^2-M_Y^2)}{4M_Y M_N}\right]\phi_{\rm SO}^0\cdot\tfrac{1}{2}(\boldsymbol{\sigma}_1-\boldsymbol{\sigma}_2)\cdot\mathbf{L}+\frac{1}{4M_Y M_N}(\nabla^2\phi_C^0+\phi_C^0\nabla^2)\right\}\Bigg]P\ .\end{aligned} \tag{39}$$

(d) Diffractive exchange:

$$\begin{aligned}V_D(r)=\frac{m_p}{4\pi}\Bigg[&g_{13}^D g_{24}^D\frac{4}{\sqrt{\pi}}\frac{m_P^2}{\mathcal{M}^2}\cdot\left\{\left\{1+\frac{m_P^2}{2M_Y M_N}(3-2m_P^2r^2)+\frac{m_P^2}{M_Y M_N}\mathbf{L}\cdot\mathbf{S}+\left[\frac{m_P}{2M_Y M_N}\right]^2 Q_{12}\right.\right.\\&\left.+\frac{m_P^2}{M_Y M_N}\left[\frac{(M_N^2-M_Y^2)}{4M_Y M_N}\right]\cdot\tfrac{1}{2}(\boldsymbol{\sigma}_1-\boldsymbol{\sigma}_2)\cdot\mathbf{L}\right\}e^{-m_P^2r^2}\\&\left.+\frac{1}{4M_Y M_N}(\nabla^2 e^{-m_P^2r^2}+e^{-m_P^2r^2}\nabla^2)\right\}\Bigg]P\ .\end{aligned} \tag{40}$$

In these formulas m is the average mass in the meson isospin multiplet.

V. MULTICHANNEL SCHRÖDINGER EQUATION

We have to solve the Lippmann-Schwinger for the *YN* reactions:

$$\begin{aligned}&\text{(I)}\ \ \Sigma^+p\to\Sigma^+p\ ,\\ &\text{(II)}\ \ (\Lambda p,\Sigma^+n,\Sigma^0p)\to(\Lambda p,\Sigma^+n,\Sigma^0p)\ ,\\ &\text{(III)}\ \ (\Lambda n,\Sigma^0n,\Sigma^-p)\to(\Lambda n,\Sigma^0n,\Sigma^-p)\ .\end{aligned}\tag{41}$$

So, reaction (I) involves only a single two-particle channel, but for (II) and (III) the state vectors $|\psi)$ are three-component vectors and the potentials V are 3×3 matrices in the two-particle channel space. For system (II) we have on the physical particle basis

$$|\psi)_{\rm II}=\begin{bmatrix}|\psi)_{\Lambda p}\\ |\psi)_{\Sigma^+n}\\ |\psi)_{\Sigma^0p}\end{bmatrix},\quad V_{\rm II}=\begin{bmatrix}V_{\Lambda\Lambda} & V_{\Lambda\Sigma^+} & V_{\Lambda\Sigma^0}\\ V_{\Sigma^+\Lambda} & V_{\Sigma^+\Sigma^+} & V_{\Sigma+\Sigma^0}\\ V_{\Sigma^0\Lambda} & V_{\Sigma^0\Sigma^+} & V_{\Sigma^0\Sigma^0}\end{bmatrix},\tag{42}$$

and likewise for system (III) we have

$$|\psi)_{\rm III}=\begin{bmatrix}|\psi)_{\Lambda n}\\ |\psi)_{\Sigma^0n}\\ |\psi)_{\Sigma^-p}\end{bmatrix},\quad V_{\rm III}=\begin{bmatrix}V_{\Lambda\Lambda} & V_{\Lambda\Sigma^0} & V_{\Lambda\Sigma^-}\\ V_{\Sigma^0\Lambda} & V_{\Sigma^0\Sigma^0} & V_{\Sigma^0\Sigma^-}\\ V_{\Sigma^-\Lambda} & V_{\Sigma^-\Sigma^0} & V_{\Sigma^-\Sigma^-}\end{bmatrix},\tag{43}$$

where $V_{\Lambda\Sigma^+}=(\Lambda p|V|\Sigma^+n)$, etc. In the case of exact isospin symmetry of the potential the matrices $V_{\rm II}$ and V_{III} are connected by an isospin rotation.

Expressing the potentials on the physical particle basis in the potential matrix elements on the isospin basis, we find for (II)

$$V_{\rm II}=\begin{bmatrix}V_{\Lambda\Lambda} & \sqrt{\tfrac{2}{3}}V_{\Lambda\Sigma} & -\sqrt{\tfrac{1}{3}}V_{\Lambda\Sigma}\\ \sqrt{\tfrac{2}{3}}V_{\Lambda\Sigma} & \tfrac{1}{3}[2V_{\Sigma\Sigma}(\tfrac{1}{2})+V_{\Sigma\Sigma}(\tfrac{3}{2})] & \frac{\sqrt{2}}{3}[-V_{\Sigma\Sigma}(\tfrac{1}{2})+V_{\Sigma\Sigma}(\tfrac{3}{2})]\\ -\sqrt{\tfrac{1}{3}}V_{\Lambda\Sigma} & \tfrac{2}{3}[-V_{\Sigma\Sigma}(\tfrac{1}{2})+V_{\Sigma\Sigma}(\tfrac{3}{2})] & \tfrac{1}{3}[V_{\Sigma\Sigma}(\tfrac{1}{2})+2V_{\Sigma\Sigma}(\tfrac{3}{2})]\end{bmatrix},\tag{44}$$

and for (III)

$$V_{\rm III}=\begin{bmatrix}V_{\Lambda\Lambda} & \sqrt{\tfrac{1}{3}}V_{\Lambda\Sigma} & -\sqrt{\tfrac{2}{3}}V_{\Lambda\Sigma}\\ \sqrt{\tfrac{1}{3}}V_{\Lambda\Sigma} & \tfrac{1}{3}[V_{\Sigma\Sigma}(\tfrac{1}{2})+2V_{\Sigma\Sigma}(\tfrac{3}{2})] & \frac{\sqrt{2}}{3}[-V_{\Sigma\Sigma}(\tfrac{1}{2})+V_{\Sigma\Sigma}(\tfrac{3}{2})]\\ -\sqrt{\tfrac{2}{3}}V_{\Lambda\Sigma} & \frac{\sqrt{2}}{3}[-V_{\Sigma\Sigma}(\tfrac{1}{2})+V_{\Sigma\Sigma}(\tfrac{3}{2})] & \tfrac{1}{3}[2V_{\Sigma\Sigma}(\tfrac{1}{2})+V_{\Sigma\Sigma}(\tfrac{3}{2})]\end{bmatrix}.\tag{45}$$

In Table I we give the channels and states relevant to this work and in anticipation of the further discussions, we also give here the SU(3) contents of the potentials on the isospin basis.

The multichannel Lippmann-Schwinger equation for the components of the state vector $\tilde{\psi}_i(\mathbf{q}_i)$ corresponding to Eq. (9) reads

$$\tilde{\psi}_i(\mathbf{q}_i)=\tilde{\phi}_i(\mathbf{q}_i)+2M_{n_1,n_2}\sum_n\int\frac{d^3k_n}{(2\pi)^3}\frac{1}{\mathbf{q}_n^2-\mathbf{k}_n^2+i\varepsilon}(i_1,i_2|V|n_1,n_2)\tilde{\psi}_n(\mathbf{q}_n)\ .\tag{46}$$

The multichannel Schrödinger equation in configuration space is derived from the Lippmann-Schwinger equation through the standard Fourier transformation (see, for example, Ref. 1). We find

$$\sum_j\{(-2\mu_i)^{-1}\delta_{i,j}\nabla^2+V_{i,j}(r)-[\nabla^2\phi_{i,j}(r)+\phi_{i,j}(r)\nabla^2]+M_i\delta_{i,j}\}\psi_j(r)=E_i\psi_i(r)\ .\tag{47}$$

Here μ_i stands for the reduced mass in channel i, i.e., $M_{i,j}=\mu_i\delta_{i,j}$, $M_i=M_{i_1}+M_{i_2}$ is the total rest mass for channel i, and E is the total energy in the center of mass. By $V_{i,j}(r)$ is meant the local part of the potentials, i.e., all terms in Eq. (27) but the last one.

We make the partial-wave projection of Eq. (47) and write for the partial wave $\psi^{\rm LSJ}_{M,i}=\Sigma C^{\rm LSJ}_{m\mu M}(u_{l,i}/r)Y^{(l)}_m\chi^{(S)}_\mu$ Introducing the center-of-mass momentum $k_i^2=2\mu_i(E-M)_i$, and defining $f_{i,j}(r)=\mu_{i,i}\phi_{i,j}(r)$, we get from Eq. (47) for the radial Schrödinger equation

TABLE I. SU(3) contents of the various potentials on the isospin basis.

Space-spin antisymmetric states $^1S_0$, ^3P, $^1D_2$, ...		
$NN\to NN$	$I=1$	$V_{NN}(I=1)=V_{27}$
$\Lambda N\to\Lambda N$		$V_{\Lambda\Lambda}(I=\frac{1}{2})=(9V_{27}+V_{8s})/10$
$\Lambda N\to\Sigma N$	$I=\frac{1}{2}$	$V_{\Lambda\Sigma}(I=\frac{1}{2})=(-3V_{27}+3V_{8s})/10$
$\Sigma N\to\Sigma N$		$V_{\Sigma\Sigma}(I=\frac{1}{2})=(V_{27}+9V_{8s})/10$
$\Sigma N\to\Sigma N$	$I=\frac{3}{2}$	$V_{\Sigma\Sigma}(I=\frac{3}{2})=V_{27}$
Space-spin symmetric states $^3S_1$, $^1P_1$, ^3D, ...		
$NN\to NN$	$I=0$	$V_{NN}(I=0)=V_{10^*}$
$\Lambda N\to\Lambda N$		$V_{\Lambda\Lambda}(I=\frac{1}{2})=(V_{10^*}+V_{8a})/2$
$\Lambda N\to\Sigma N$	$I=\frac{1}{2}$	$V_{\Lambda\Sigma}(I=\frac{1}{2})=(V_{10^*}-V_{8a})/2$
$\Sigma N\to\Sigma N$		$V_{\Sigma\Sigma}(I=\frac{1}{2})=(V_{10^*}+V_{8a})/2$
$\Sigma N\to\Sigma N$	$I=\frac{3}{2}$	$V_{\Sigma\Sigma}(I=\frac{3}{2})=V_{10}$

$$(\delta_{i,j}+2f_{i,j})\left[u''_{l,j}-\frac{l(l+1)}{r^2}u_{l,j}\right]+2f'_{i,j}u'_{l,i}+[k_i^2\delta_{i,j}-(2\mu_i V_{i,j}+f''_{i,j})]u_{l,j}=0\ , \quad (48)$$

which we put into the form

$$N\left[u''-\frac{l(l+1)}{r^2}u\right]+N'u'+Au+\tfrac{1}{2}N''u=0\ . \quad (49)$$

We now transform away the u' term in the standard way, by writing

$$u=Tv\ , \quad (50)$$

where the transformation matrix T satisfies the differential equation

$$2NT'+N'T=0\ , \quad (51)$$

with the boundary condition $T\to 1$ for $r\to\infty$. As a result $v(r)$ satisfies an ordinary local multichannel Schrödinger equation

$$v_l''+\left[k^2-2M_{\rm red}W-\frac{l(l+1)}{r^2}\right]v_l=0\ , \quad (52)$$

where the "potential" W in this equation is given by

$$2M_{\rm red}W=(NT)^{-1}(2M_{\rm red}V)T+\tfrac{1}{2}(NT)^{-1}(N'T')-[(NT)^{-1}k^2T-k^2] \quad (53)$$

and $(M_{\rm red})_{i,j}=\mu_i\delta_{i,j}$. This is the multichannel analogon of Eq. (39) of Ref. 1.

The differential equation for the transformation T has to be solved numerically. After T is computed we can solve the coupled-channel Schrödinger equation. For further details of handling the Schrödinger equation for coupled channels we refer to Refs. 15 and 23.

VI. FORM FACTORS AND SU(3)

The states of SU(3) irreps for the NN channels and in particular the YN channels, are displayed in Table II. The partial connection between the YN and NN channels via SU(3) is evident from this table.

We assume that SU(3) symmetry is broken only kinematically, i.e., via the physical masses of the mesons and baryons. In Ref. 7 the SU(3) irreps in the BB channels form the basis for the parametrization of the short-range interaction with "hard cores." Here we follow the same scheme except that the role of the "hard cores" is taken over by the form factors. The behavior of these form factors is controlled by Λ, the so-called cutoff mass [see Eq. (21)]. Thus for the S waves the cutoff masses of the $\{27\}$ and the $\{10^*\}$ are in principle fixed in the NN fit. In YN we then have as free-form-factor parameters the $\{8_s\}$-, $\{8_a\}$-, and the $\{10\}$-cutoff masses. However, because of the various SU(3)-symmetry-breaking mechanisms included in the model, we are forced to calculate the nuclear potentials on the isospin basis. On this level, we not only have to deal with states belonging to a single SU(3) irrep, but also with states belonging to a combination of two irreps (see Table II). In the latter case, we than allow for a separate form factor. Altogether, this would imply four different form factors to be used:

Λ_{27} for $^1S_0(\Sigma N;\ I=\frac{3}{2})$,

Λ_{10} for $^3S_1(\Sigma N;\ I=\frac{3}{2})$,

Λ_{27+8_s} for $^1S_0(\Lambda N,\Sigma N;\ I=\frac{1}{2})$,

$\Lambda_{10^*+8_a}$ for $^3S_1(\Lambda N,\Sigma N;\ I=\frac{1}{2})$.

Note that in the ΛN and ΣN isospin $I=\frac{1}{2}$ channels the SU(3) irreps have different weights (see Table I). Therefore it is justified to use different form-factor masses for these cases. However, in order to obtain a good fit this was unnecessary.

The S waves are by far the dominant waves for fitting the low-energy YN data, which are mainly total cross sections. The P waves are not very important for the latter and so from these data the experimental P-wave information is meagre. Also from the measured low-energy differential cross sections there is no evidence for large P waves. It appeared that we could use the same form factor for states with different L, but in isomorphic SU(3) ir-

TABLE II. Channels, states, and SU(3) irreps in $Y=1$ and $Y=2$ baryon-baryon scattering.

Y	I	Channels	States	SU(3) irreps
2	1	NN	$^1S_0$, ^3P, $^1D_2$, ...	$\{27\}$
	0		$^3S_1$, $^1P_1$, ^3D, ...	$\{10^*\}$
1	$\frac{1}{2}$	$\Lambda N,\Sigma N$	$^1S_0$, ^3P, $^1D_2$, ...	$\{27\}\oplus\{8_s\}$
			$^3S_1$, $^1P_1$, ^3D, ...	$\{10^*\}\oplus\{8_a\}$
	$\frac{3}{2}$	ΣN	$^1S_0$, ^3P, $^1D_2$, ...	$\{27\}$
			$^3S_1$, $^1P_1$, ^3D, ...	$\{10\}$

TABLE III. S-wave form-factor masses used in this work.

$^1S_0$	Σ^+p	$\{27\}$	$\Lambda_{27}=1020.0$ MeV
$^3S_1$	Σ^+p	$\{10\}$	$\Lambda_{10}=1230.0$ MeV
	Σ^-p	$\{10\}$	$\Lambda'_{10}=1270.5$ MeV
$^1S_0$	$\Lambda N,\Sigma N$	$\{27\}+\{8_s\}$	$\Lambda_{27+8_s}=820.0$ MeV
$^3S_1$	$\Lambda N,\Sigma N$	$\{10^*\}+\{8_a\}$	$\Lambda_{10^*+8_a}=1270.5$ MeV

reps, without giving any problems with the data at higher energies.

It turned out that imposing a form-factor assignment on the basis of strict SU(3) symmetry leads to a certain friction between the Σ^+p and the Σ^-p channels for the $^3S_1$ wave. The capture ratio at rest and the Σ^-p cross sections are very sensitive to the potential in the $\{10\}$. In order to fit these data we would have to allow for a cutoff mass Λ in the $\{10\}$ such that the model would produce an unobserved bound state in the $^3S_1$ Σ^+p state. To avoid this, we take a separate form factor for the $^3S_1$ Σ^+p and $^3S_1$ Σ^-p $I=\frac{3}{2}$ states. This means that we introduce an SU(2) breaking for the irrep $\{10\}$. This breaking could not be explained by refining our CSB treatment, i.e., by including the $\pi-\eta$ and $\rho-\omega$ mixing. These effects turned out to be very small. Also, introducing a breaking of the π^0 coupling[24] could not solve this.

The amount of SU(2) breaking needed could also be varied by allowing a medium strong SU(3) breaking in the $\{27\}$ form factor, i.e., not taking the value of Λ_{27} as found in NN. This could be justified by arguing that in the YN channels, $Y\neq 0$ exchange occurs, which introduces some medium strong SU(3)-breaking effects also in the form factor masses. However, this way we cannot eliminate the SU(2) breaking completely. The Σ^-p data force the Λ_{10} in a region where the $^3S_1$ is very sensitive to a possible SU(2) breaking. We now have two choices: (i) we make the SU(2) breaking in the $\{10\}$ as small as possible at the cost of an SU(3) breaking for Λ_{27}, or (ii) we keep strict SU(3) for Λ_{27} and introduce a larger SU(2) breaking for the Λ_{10}. In principle we have no clear reason to prefer (i) or (ii). The model (coupling constants, etc.) and the fit to the data do not depend on the choice made here. In the following we will work with choice (i). The results for choice (ii) are very similar. Although (ii) would be more appealing [one parameter less and strict SU(3) in the Λ_{27}], it appears that then the $^3S_1$ wave in the Σ^+p becomes more repulsive and this seems to be unfavorable for the Σ hyperfragments.[25]

In Table III we finally summarize the form-factor prescription as used in the calculations [choice (i), as previously stated] and give the form-factor masses which have emerged from the YN fit. As one sees from the table, our form-factor scheme is finally very simple: (i) for Σ^+p a $^1S_0$ and a $^3S_1$ form factor, (ii) for $\Lambda N-\Sigma N$ a $^1S_0$ and a $^3S_1$ form factor.

VII. COUPLING CONSTANTS, $F/(F+D)$ RATIOS, AND MIXING ANGLES

The OBE-coupling constants we employ here for the description of the YN channels are obtained from the NN analysis of Ref. 1 using SU(3) relations. The SU(3) relations are assumed to hold for the pseudovector couplings of the pseudoscalar mesons, for the Pauli-Dirac couplings of the vector mesons, for the coupling of the scalar mesons, and for the Pomeron and tensor-meson contributions. We have analyzed the low-energy YN data (see, e.g., Refs. 6, 7, 15, and 23 for a description) for all YN channels simultaneously. An excellent solution was found which appears qualitatively even better than the Nijmegen hard-core potentials.[6,7] The handling of SU(3) for the pseudoscalar and vector mesons has been discussed in Refs. 7 and 13. Here we briefly discuss the treatment of the scalar mesons and the "diffractive" exchange.

In the scalar-meson nonet the physical ε and S^* meson are described in terms of the SU(3) singlet ε_0 and octet state S_0^* using a single mixing angle θ_S

$$\begin{aligned}|\varepsilon\rangle&=\cos\theta_S|S_0^*\rangle-\sin\theta_S|\varepsilon_0\rangle\ ,\\ |S^*\rangle&=\sin\theta_S|S_0^*\rangle+\cos\theta_S|\varepsilon_0\rangle\ .\end{aligned}\tag{54}$$

With this convention, the ideal mixing angle for the scalar mesons in the $q^2\bar{q}^2$ picture[26] is $\theta_S=35.3°$, and in the $q\bar{q}$ picture is $\theta_S=54.7°$.[27] The convention Eq. (54) differs from that in Ref. 7. There the same convention is used as for the vector and pseudoscalar mesons (for definitions see Refs. 5 and 6). For the vector and pseudoscalar mesons we stick to the conventions used in Refs. 5 and 6. Using these expressions for meson mixing the couplings can readily be expressed in terms of the singlet coupling g_1, the octet coupling g_8, the $F/(F+D)$ ratio α_S, and the mixing angle θ_S.

For the "diffractive" exchanges we take the "bare" Pomeron as an SU(3) singlet. The tensor nonet contains the f_0 and the f'_0 which are, respectively, the SU(3) singlet and octet state. Exact SU(3) and unitarity cause a strong mixing between the "bare" Pomeron and f_0. We describe this system by P_0, which is obviously a SU(3) singlet. Medium strong SU(3) breaking then gives mixing of P_0 and f'_0, leading to the physical Pomeron P and f. In the NN analysis the combination

$$g_P^2=g_{PNN}^2+g_{fNN}^2=g_1^2+\tfrac{1}{3}(4\alpha_D-1)^2g_8^2\ ,\tag{55}$$

and also $g_8=g_{A_2NN}$ has been fixed. From the expression for g_P^2 one sees that g_1 and α_D can be written in terms of g_P, g_{A_2NN}, and an angle that we call ψ_D. One has

$$\begin{aligned}g_1&=\cos(\psi_D)g_P\ ,\\ (4\alpha_D-1)/\sqrt{3}&=\sin(\psi_D)g_P/g_{A_2NN}\ .\end{aligned}\tag{56}$$

So, in the YN analysis we have for the diffractive contributions one extra free parameter, the angle ψ_D. Another possible relevant free parameter would be θ_D, but since we have used the same mass m_P for all diffractive exchanges, we have no SU(3) breaking due to these exchanges and so the results are independent of θ_D. In Ref. 3 a natural kinematical SU(3) breaking is suggested in $\Delta(\mathbf{k}^2,m^2)$ by using in Eq. 22 M_YM_N instead of $\mathcal{M}^2$ in the denominator. However, a recent analysis of the Pomeron

TABLE IV. Coupling constants for pseudoscalar and vector meson $Y=0$ and $Y=\pm 1$ exchanges.

M		NNM	$\Lambda\Lambda M$	$\Lambda\Sigma M$	$\Sigma\Sigma M$	ΛNM	ΣNM
π	g	3.698 22	CSB	3.383 18	3.328 40		
	f	0.272 04	CSB	0.202 61	0.193 15		
η	g	1.805 74	−1.849 05		4.456 48		
η'	g	1.958 94	4.025 37		1.567 18		
K	g					−3.981 22	1.207 49
	f					−0.964 66	0.283 36
ρ	g	0.891 47	CSB		1.782 95		
	f	3.762 55	CSB	3.149 85	2.069 40		
ϕ	g	−0.314 77	−1.539 76		−1.539 76		
	f	−0.424 14	−3.095 42		1.902 46		
ω	g	2.946 63	2.006 66		2.006 66		
	f	0.909 59	−1.140 16		2.694 85		
K^*	g					−1.544 08	−0.891 47
	f					−3.367 08	1.693 15

couplings[28] suggests that there is almost no SU(3) breaking of this kind.

In Tables IV and V we have listed the coupling constants. All figures refer to rationalized couplings, i.e., they should be understood as $g/\sqrt{4\pi}$. Furthermore "CSB" refers to the couplings due to charge symmetry breaking and are given by $g_{\Lambda\Lambda M}(\mathrm{CSB}) = -0.0271 g_{NNM} g_{\Lambda\Sigma M}$.

The value found for α_{PV} agrees very well with the determination in weak interactions.[12,13] The advantage of our combined NN and YN analysis, in contrast to most other analyses, is that α_{PV} enters in many coupling constants simultaneously ($NN\eta_8$, $\Sigma\Sigma\pi$, $\Lambda\Sigma\pi$, ΛNK, ΣNK, $\Lambda\Lambda\eta_8$, and $\Sigma\Sigma\eta_8$) and is vital to several measured cross sections and ratios. Also, the value obtained for α_V^m is in full accordance with relativistic SU(6).[14] Note that here α_V^e has not been fitted, but is theoretical input. Another important free parameter is the scalar mixing angle θ_S. The fit appears to be rather sensitive to this parameter, but there is still some room for variation by making at the same time adjustments for ψ_D and Λ_{10}. We obtained $\theta_S \approx 40.9°$, a value between ideal mixing for the scalar $q^2\bar{q}^2$ and the scalar $q\bar{q}$ states. In the region where the data can be fitted successfully the $\Sigma^- p$ elastic and inelastic cross sections depend rather steeply on θ_S. A recent determination of θ_S,[29] based on a study of $\Gamma(S^* \to \pi\pi)$, gave $\theta_S = 32°$. For the angle ψ_D we obtained the value 15.5°, which means that the Pomeron is dominantly an SU(3) singlet as is also found in high-energy scattering.

The singlet couplings g_1 can readily be calculated using the values of the tables and the formulas (this paper and Refs. 5 and 6) for the meson mixings.

In Table VI we give the singlet and octet coupling constants, mixing angles, and $F/(F+D)$ ratios.

For a discussion of the NNM-coupling constants we refer to Ref. 1. In the discussion of the YYM and YNM-coupling constants we shall restrict ourselves mainly to the pseudoscalar mesons, because there is independent information on them available from the application of the Goldberger-Treiman relation and the analysis of KN scattering. We compare in the following our values with those in the literature, i.e., as given in the compilations of coupling constants.[12,13]

In Refs. 12 and 13 are given $g^2_{\Sigma\Sigma\pi}/4\pi = 13\pm 2$ and $g^2_{\Lambda\Sigma\pi}/4\pi = 11\pm 1$. We have $g^2_{\Sigma\Sigma\pi}/4\pi = 11.09$ and $g^2_{\Lambda\Sigma\pi}/4\pi = 11.42$, which agree very well with those from the literature. To a certain extent, this is no surprise because (i) we have used SU(3) for the pseudovector (PV) coupling, and (ii) we found a perfect $F/(F+D)$ ratio. Pilkuhn showed[30] using the Goldberger-Treiman relation in combination with superconvergence that one can expect that only the pseudovector couplings satisfy SU(3)

TABLE V. Coupling constants for scalar meson and "diffractive" $Y=0$ and $Y=\pm 1$ exchanges.

M		NNM	$\Lambda\Lambda M$	$\Lambda\Sigma M$	$\Sigma\Sigma M$	ΛNM	ΣNM
δ	g	1.277 34	CSB	−0.421 16	3.284 16		
S^*	g	−0.838 94	−2.563 08		−3.114 53		
ε	g	4.767 73	2.776 98		2.140 25		
κ	g					−2.633 59	−2.006 82
A_2	g	0.443 72	CSB	−0.014 27	1.151 96		
f'	g	−1.109 89	−2.055 61		−2.217 79		
$P \oplus f$	g	2.747 08	2.701 61		2.866 06		
K^{**}	g					−0.814 69	−0.514 08

TABLE VI. Coupling constants, $F/(F+D)$ ratios, mixing angles, etc. The values with an asterisk have been determined in the fit to the *YN* data. The other parameters are theoretical input or determined by the fitted parameters and the constraint from the *NN* analysis.

Mesons		{1}	{8}	$F/(F+D)$	Angles
Pseudoscalar	f	0.184 55	0.272 04	$\alpha_{PV}=0.355$*	$\theta_P=-23.00°$
Vector	g	2.529 34	0.891 47	$\alpha_V^e=1.0$	$\theta_V=37.50°$
	f	0.979 82	3.762 55	$\alpha_V^m=0.275$*	
Scalar	g	3.755 48	1.277 34	$\alpha_S=1.285\,55$	$\theta_S=40.895°$*
Diffractive	g	2.855 07	0.443 72	$\alpha_D=1.022\,67$	$\psi_D=15.50°$*

very well.

From $K^{\pm}N$ forward dispersion relations one has determined the *YNK*-coupling constants. Typically one finds[12] $g^2_{\Lambda NK}/4\pi=13.9\pm2.6$ and $g^2_{\Sigma NK}/4\pi=0.9\pm0.4$. We have $g^2_{\Lambda NK}/4\pi=16.0$ and $g^2_{\Sigma NK}/4\pi=1.44$, again in good agreement. These values are also perfectly compatible with the determinations of the effective coupling

$$g_Y^2\equiv(g^2_{\Lambda NK}+0.84g^2_{\Sigma NK})/4\pi\ .$$

In Ref. 12, for example, one quotes $g_Y^2=16.6\pm0.7$, which is also close to our determination $g_Y^2=17.2$. The conclusion we draw from this comparison is that the use of SU(3) for the PV coupling has led to a seemingly perfect realistic description of the pseudoscalar meson exchange in the present model.

We close this section by making some remarks on the couplings of the vector mesons in the context of the naive nonrelativistic quark model (henceforth referred to as QM). For similar observations pertinent to model *D* (Ref. 6) and *F* (Ref. 7), see Ref. 31. Because $g_{NN\phi}/\sqrt{4\pi}=-0.31$ is fairly small and since we use ideal mixing, it is clear that the QM relations

$$g_{\Sigma\Sigma\omega}=g_{\Lambda\Lambda\omega}=\tfrac{2}{3}g_{NN\omega},\quad g_{\Sigma\Sigma\phi}=g_{\Lambda\Lambda\phi},\quad g_{NN\phi}=0 \tag{57}$$

are indeed satisfied approximately in Table IV. To illustrate further how close we obey QM relations for the electric couplings we look at

$$g_{NN\phi}=-\sin\theta_V g_1+\cos\theta_V(4\alpha_V^e-1)g_8/\sqrt{3}\ . \tag{58}$$

Imposing the QM restriction $g_{NN\phi}=0$ one gets that

TABLE VII. Comparison of the calculated and experimental values for the 35 *YN* data that were included in the fit. The superscripts *RH* and *M* denote, respectively, the Rehovoth-Heidelberg (Ref. 33) and Maryland (Ref. 34) data. The laboratory moments are in MeV/c and the total cross sections in mb.

$\Lambda p\to\Lambda p$		$\chi^2=1.0$	$\Lambda p\to\Lambda p$		$\chi^2=2.6$
p_Λ	σ_{exp}^{RH}	σ_{th}	p_Λ	σ_{exp}^{M}	σ_{th}
145	180±22	192.8	135	209.0±58	209.2
185	130±17	138.8	165	177.0±38	163.6
210	118±16	113.2	195	153.0±27	127.9
230	101±12	96.4	225	111.0±18	100.4
250	83±9	82.4	255	87.0±13	79.2
290	57±9	60.8	300	46.0±11	56.6
$\Sigma^+p\to\Sigma^+p$		$\chi^2=0.2$	$\Sigma^-p\to\Sigma^-p$		$\chi^2=2.6$
p_{Σ^+}	σ_{exp}	σ_{th}	p_{Σ^-}	σ_{exp}	σ_{th}
145	123±62	107.3	142.5	152±38	137.4
155	104±30	99.9	147.5	146±30	135.5
165	92±18	91.4	152.5	142±25	133.9
175	81±12	84.3	157.5	164±32	132.4
			162.5	138±19	131.0
			167.5	113±16	129.8
$\Sigma^-p\to\Sigma^0n$		$\chi^2=6.5$	$\Sigma^-p\to\Lambda n$		$\chi^2=2.7$
p_{Σ^+}	σ_{exp}	σ_{th}	p_{Σ^-}	σ_{exp}	σ_{th}
110	396±91	178.3	110	174±47	219.1
120	159±43	157.5	120	178±39	191.7
130	157±34	140.5	130	140±28	169.6
140	125±25	126.3	140	164±25	151.4
150	111±19	114.2	150	147±19	136.2
160	115±16	103.8	160	124±14	123.4
	$r_R^{exp}=0.468\pm0.010$			$r_R^{th}=0.471$	$\chi^2=0.1$

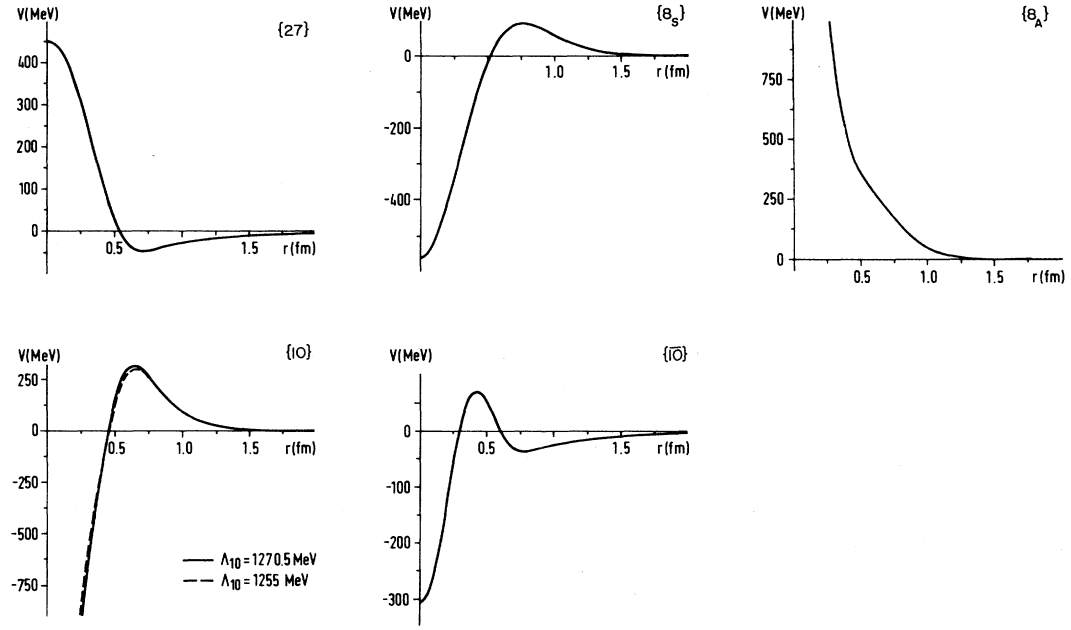

FIG. 1. Potentials for channels in definite SU(3).

$$\frac{g_1}{g_8\sqrt{6}}\sqrt{2}\tan\theta_V = 1 \ . \tag{59}$$

From Table VI we find for this combination 1.26, which is rather close to the QM value. Models D and F here give 2.34 and 1.75, respectively.[31]

For the magnetic couplings $G^m=(f+g)$ one would have $\alpha_V^m=\frac{2}{5}$ following static SU(6), whereas we have the relativistic SU(6) value.[14] The QM would require, using $\alpha_V^m=\frac{2}{5}$, that $G_1^m/G_8^m\sqrt{6}=\frac{1}{5}$ and we have for this combination 0.308. Models D and F give here, respectively, 0.423 and 0.255.

Usually OBE models have larger relative strengths for the tensor couplings of vector mesons than the QM (see, e.g., Refs. 12 and 13). In this respect the present soft-core model is closer to the QM than other models. Note

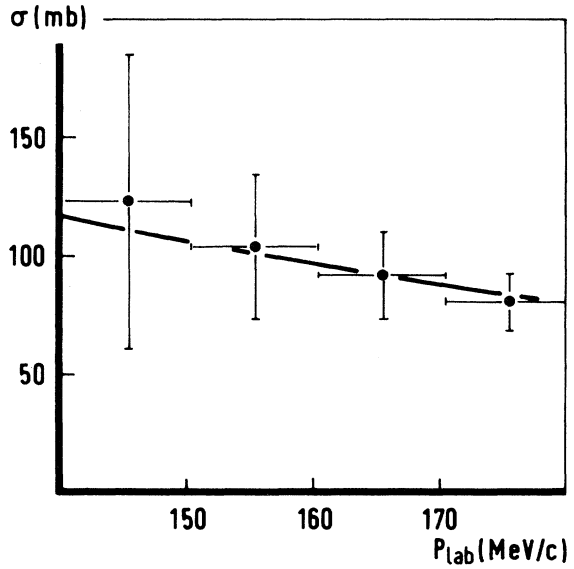

FIG. 2. Calculated Σ^+p "total" cross sections compared with experimental values of Ref. 35.

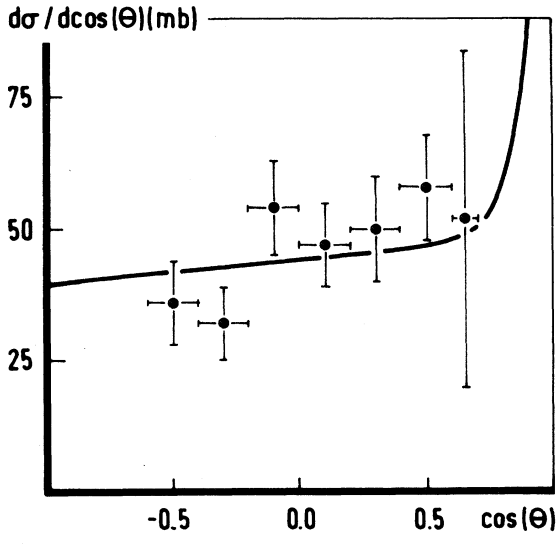

FIG. 3. Calculated Σ^+p differential cross sections compared with experimental values of Ref. 35.

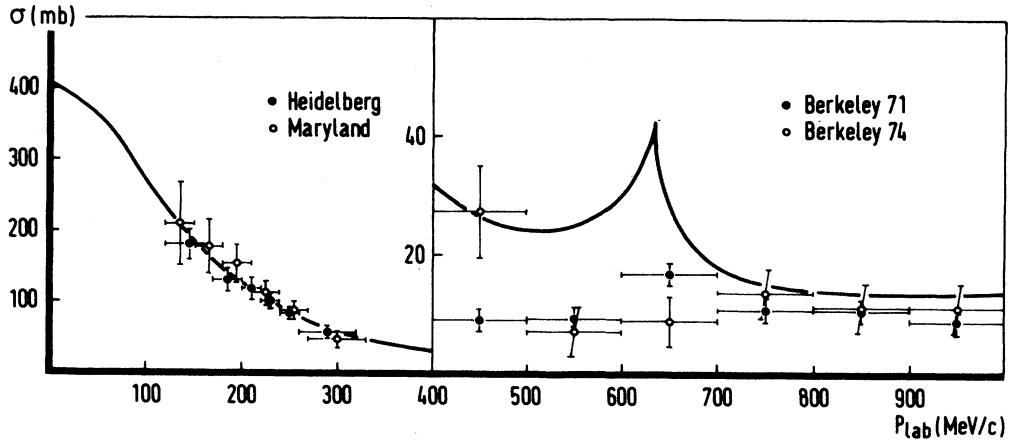

FIG. 4. Calculated Λp elastic total cross sections compared with the Rehovoth-Heidelberg (Ref. 33), Maryland (Ref. 34), and Berkeley (Refs. 39 and 40) data.

that $(f/g)_{NN\rho}=4.2$, where the QM predicts for this ratio 3.7. For the other ratios we have $(f/g)_{NN\omega}=0.31$, $(f/g)_{\Lambda NK^*}=2.2$, and $(f/g)_{\Sigma NK^*}=-1.9$. These values are closer to the QM than those for the models *D* and *F*.

VIII. RESULTS OF THE CALCULATIONS

A. Determination of the free parameters

The values for the eight free parameters in the soft-core model are determined in the *YN* analysis in a parameter search to a selected set of 35 best low-energy *YN* data (Table VII, the data are from Refs. 32–37). The fitted parameters and the values obtained are given in Tables IV and V.

The lowest total $\chi^2=15.7$ reached for the 35 data and 8 free parameters, i.e., χ^2 per degree of freedom $=0.58$. In Table VII we compare the calculated model values with the experimental ones. In calculating the cross sections the *P*-wave contributions have been included. (Note here that the $^1P_1$-$^3P_1$ transitions are not included in our calculations.) In counting the number of free parameters we could have been less conservative and say that α_{PV} and α_V^m are fixed during the search. After we noticed that we could fix these parameters on the "theoretical" ideal values, we did not allow them to vary. So actually we

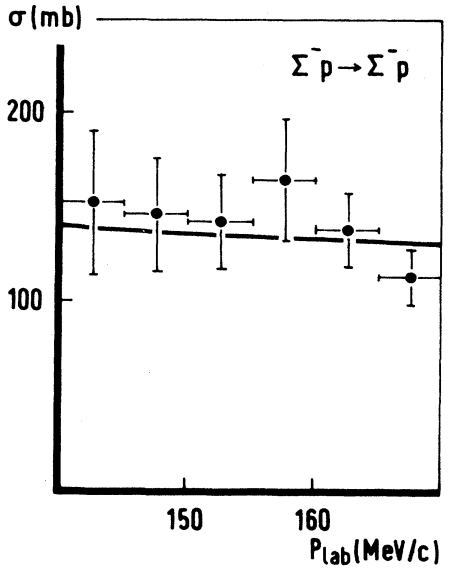

FIG. 5. Calculated $\Sigma^- p$ "total" cross sections compared with experimental data (Ref. 35).

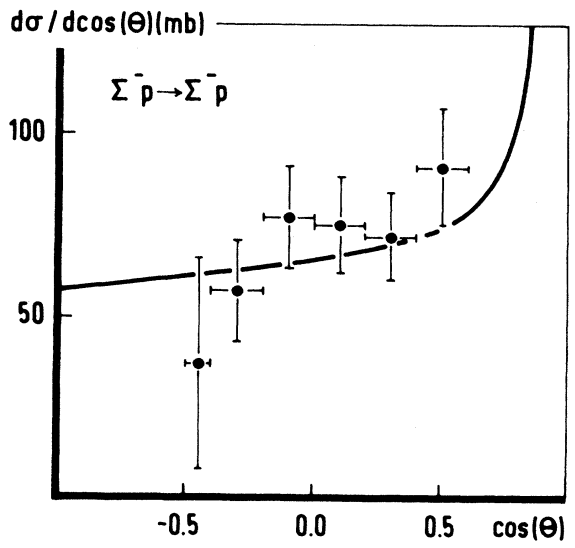

FIG. 6. Calculated $\Sigma^- p$ differential cross sections compared with experimental data (Ref. 35).

TABLE VIII. Σ^+p and Σ^-n S- and P-wave effective range parameters in units of fm. The superscript C denotes the presence of the Coulomb interaction.

	$^1S_0$	$^3S_1$	$^3P_0$	$^3P_1$	$^3P_2$	$^1P_1$
a^C	−3.63	0.305	−2.33	1.63	−0.099	−0.97
r^C	3.27	−20.15	4.77	−7.66	10.60	13.74
a	−4.71	0.247	−2.12	1.49	−0.101	−0.88
r	3.36	−26.86	4.93	−8.33	26.30	14.56

TABLE IX. Σ^+p nuclear bar phase shifts in degrees.

p_{Σ^+} (MeV/c)	200	400	600	800	1000
T_{lab} (MeV)	16.7	65.5	142.8	244.0	364.5
$^1S_0$	36.63	27.13	12.82	−10.05	−13.59
$^3S_1$	−7.95	−10.46	6.51	40.70	51.17
ε_1	−1.83	−4.24	−2.31	3.74	5.80
$^3P_0$	4.42	7.53	0.80	−10.31	−22.35
$^1P_1$	1.71	4.27	4.10	1.06	−3.61
$^3P_1$	−3.14	−10.40	−18.46	−26.86	−34.90
$^3P_2$	0.54	3.14	6.61	10.81	15.91
ε_2	−0.35	−1.80	−2.90	−2.85	−1.67
$^3D_1$	0.27	1.14	0.81	−1.67	−7.25
$^1D_2$	0.28	1.64	3.93	6.59	8.52
$^3D_2$	−0.43	−2.43	1.08	1.10	0.21
$^3D_3$	0.03	0.46	−5.11	−8.57	−12.91

TABLE X. Λp and Λn S- and P-wave effective range parameters in units of rm.

		$^1S_0$	$^3S_1$	$^3P_0$	$^3P_1$	$^3P_2$	$^1P_1$
Λp	a	−2.73	−1.48	−0.033	0.016	−0.200	0.088
	r	2.87	3.04	−154	2887	11.62	−38.5
ΛN	a	−2.78	−1.41	−0.096	0.061	−0.20	0.062
	r	2.88	3.11	72.3	40.86	10.44	32.7
Λn	a	−2.86	−1.24	−0.156	0.108	−0.199	0.037
	r	2.91	3.33	62.6	−42.1	9.62	388

TABLE XI. Λp nuclear bar phase shifts in degrees below the ΣN thresholds.

p_Λ (MeV/c)	100	200	300	400	500	600	633.4
T_{lab} (MeV)	4.5	17.8	39.6	69.5	106.9	151.1	167.3
$^1S_0$	27.43	33.47	30.13	23.78	16.61	9.47	7.21
$^3S_1$	17.08	24.78	26.07	25.32	25.68	33.36	51.97
ε_1	0.20	1.15	2.91	5.61	9.83	18.31	27.78
$^3P_0$	0.03	0.12	−0.09	−1.30	−3.79	−7.30	−8.56
$^1P_1$	−0.06	−0.40	−1.25	−2.70	−4.70	−6.59	−7.74
$^3P_1$	−0.02	−0.26	−1.03	−2.47	−4.49	−6.69	−7.20
$^3P_2$	0.14	0.95	2.61	4.78	6.99	8.99	9.61
ε_2	0.00	−0.01	−0.07	−0.24	−0.50	−0.83	−0.98
$^3D_1$	0.00	0.05	0.31	1.06	2.79	6.69	8.51
$^1D_2$	0.00	0.04	0.28	0.90	1.93	3.27	3.76
$^3D_2$	0.00	0.07	0.38	1.10	2.29	3.89	4.51
$^3D_3$	0.00	0.03	0.19	0.57	1.18	1.92	2.18

TABLE XII. $\Lambda p \to \Lambda p, \Sigma^+ n, \Sigma^0 p$ total cross sections in mb above the ΣN thresholds.

p_Λ (MeV/c)	T_{lab} (MeV)	$\Lambda p \to \Lambda p$	$\Lambda p \to \Sigma^+ n$	$\Lambda p \to \Sigma^0 p$
650	175.5	26.20	6.29	2.49
700	201.4	17.02	7.94	4.18
750	228.7	14.48	8.37	4.27
800	257.2	13.56	8.21	4.11
850	286.9	13.32	7.82	3.88
900	317.8	13.40	7.36	3.64
950	349.7	13.62	6.90	3.40
1000	382.6	13.92	6.47	3.19

have effectively six free parameters. The potentials in the different SU(3) irreps are shown in Fig. 1. Combining these figures with Table I gives a qualitative picture of the potentials in the different isospin channels.

B. $\Sigma^+ p, \Sigma^- n$ scattering

The $\Sigma^+ p$ "total" cross sections[35] (for the definition see Ref. 23) are compared with the experimental values in Table VII and Fig. 2.

The calculated cross sections agree very well with the experimental data. The angular distribution at $p_{\Sigma^+} = 170$ MeV/c is shown in Fig. 3. This distribution has $\chi^2 = 5.0$ for seven data points. The spin singlet Coulomb interference is about three times larger in magnitude than the triplet Coulomb interference, giving in total a destructive Coulomb-interference result. In the overall result for the angular distribution this is partially compensated by the $^1S_0$-$^1P_1$ interference term. The scattering lengths and effective ranges in the S and P waves are given in Table VIII. The $^1S_0$ scattering lengths and effective ranges are similar to those of model D (Ref. 6) and model F (Ref. 7). The $^3S_1$ low-energy parameters are similar to those of model D. In model F there is more repulsion. It was found by Yamamoto and Bando[25] and by Dover and Gal[31] that model D is favored over model F as far as the ΣN potential well depths are concerned. So the present soft-core model seems to meet the requirements from the potential well depths calculations.

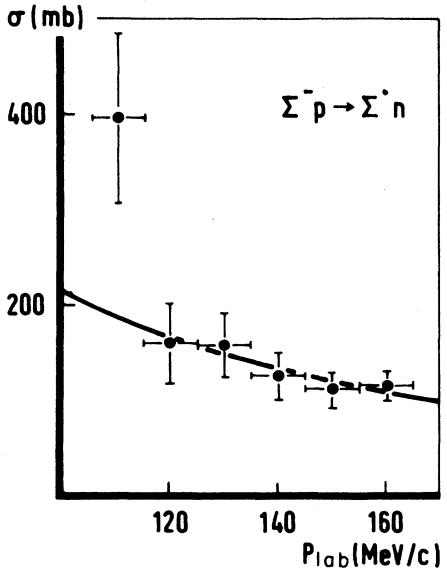

FIG. 7. Calculated $\Sigma^- p \to \Sigma^0 n$ total cross sections compared with experimental data (Ref. 32).

In Table IX the nuclear bar phase shifts for $\Sigma^+ p$ are listed. We note the great difference between the $^3S_1$ phases from the soft-core model and models D and F. This difference is caused by the attraction in the potential for $r < 0.5$ fm for the $\{10\}$ (cf. Fig. 2). In D and F this attraction was masked by the hard cores and so only the medium- and long-range repulsion was visible. Changing the cutoff Λ in the $\{10\}$ from 1230.0 to 1000.0 MeV/c the scattering length a_t ($^3S_1$) ranges from 0.31 to 0.70 fm. This way the sign change in the $^3S_1$ phase shift could be shifted to higher energies, while keeping a good fit to the $\Sigma^+ p$ total cross sections through an adjustment of the cutoff in the $\{27\}$. However, then the fit to the $\Sigma^- p$ cross sections tends to deteriorate, in particular if we make Λ_{10} too small. Note that in this case the $^3S_1$ wave is more repulsive and this makes this solution perhaps less attrac-

TABLE XIII. Inverse-scattering-length and effective-range matrices at the $\Sigma^0 p$ and $\Sigma^- p$ thresholds. The order of the states (1–4) reads $\Lambda p(^3S_1)$, $\Lambda p(^3D_1)$, $\Sigma^+ n(^3S_1)$, $\Sigma^0 p(^3S_1)$, and $\Lambda n(^3S_1)$, $\Lambda n(^3D_1)$, $\Sigma^0 n(^3S_1)$, $\Sigma^- p(^3S_1)$, respectively. The dimensions of the matrix elements are in fm$^{-1+l-l'}$ (A^{-1}) and fm$^{1-l-l'}$(R). The subscript C denotes the presence of the Couloumb interaction in the $\Sigma^- p$ channel.

	$\Lambda p \to \Sigma^0 p$		$\Lambda n \to \Sigma^- p$		$(\Lambda n \to \Sigma^- p)_C$	
	A^{-1}	R	A^{-1}	R	A^{-1}	R
11	12.33	57.22	9.73	35.00	9.74	35.16
12	−31.88	−95.73	−26.03	−53.15	−26.38	−54.82
13	−1.45	−6.29	−0.83	−3.57	−0.73	−2.64
14	1.07	3.92	1.00	2.18	1.11	2.92
22	92.20	112.86	80.85	37.96	82.52	41.66
23	1.08	15.04	0.16	8.50	−0.09	6.89
24	−0.83	−9.35	0.20	−7.06	−0.04	−8.75
33	0.24	−0.62	−0.34	−2.77	−0.27	−2.45
34	−0.78	−3.81	−0.74	−3.29	−0.69	−2.97
44	−0.27	−3.53	0.23	−1.04	−0.39	−0.71

tive for the calculation of the Σ hyperfragments.[25]

The P waves are not fitted in the soft-core model to the angular distributions; they are straightforward predictions. This in contrast to the P waves in models D and F. The triplet P waves are similar to those from D and F, which is not surprising because all models fit the NN phase shifts and both the NN and the ΣN triplet P waves are in the {27}. The $^1P_1$ phase shifts are rather moderate. This in contrast to the behavior of the $^1P_1$ in D and F.

C. ΛN scattering

The low-energy parameters of the S waves are given in Table X. In the soft-core model we clearly have $|a_s| > |a_t|$. Compared to models D and F $|a_s|$ and $|a_t|$ have become larger and smaller, respectively. The effective range r_s is reduced whereas r_t is about the same. The consequences of this for the hypertriton $^3_\Lambda$H are unclear. The effects of the changes in the scattering lengths and effective ranges can compensate each other to a certain extent.[38] Note that in our ΛN calculations we get different values for the low energy parameters in the charge +1 and 0 states, notably because of the inclusion of charge-symmetry-breaking potentials.

The fit to the low-energy Λp data is even better than in models D and F. In Table VII it is shown that the six Rehovoth-Heidelberg data have $\chi^2=1.0$ and the six Maryland data have $\chi^2=2.6$.

In Fig. 4 the Λp elastic total cross sections up to $p_\Lambda=1$ GeV/c are drawn for the experimental data. The solid line is the fit with the soft-core model (for $p_\Lambda<0.4$ GeV) and the soft-core model predictions (for $p_\Lambda>0.4$ GeV). The calculated elastic cross sections above 0.6 GeV/c are very well compatible with the Berkeley-71 data.[40]

In Table XI the Λp nuclear bar shifts are given and in Table XII we show the elastic and inelastic Λp cross sections for p_Λ from 650 MeV/c to 1 GeV/c.

The large cusp of 42.5 mb at the $\Sigma^+ n$ threshold in Fig. 4 is due to the enhancement in the $^3S_1$ waves, which is caused by the coupling of the ΛN and ΣN channels and the rather strong interaction in the $^3S_1$-wave ΣN channel. This cusp is also seen in Refs. 41 and 42, where a large peak was found in the ΛN invariant mass at $E_{\text{c.m.}}=2128.7\pm0.2$ MeV and 2129.0 ± 0.4 MeV, the $\Sigma^+ n$ threshold being located at 2128.97 MeV. To analyze this cusp we made, as in Ref. 7, a multichannel effective range approximation (ERA) around the $\Sigma^0 p$ threshold, i.e.,

$$p^{L+1/2}(\bar{K}^J)^{-1}p^{L+1/2} = -A^{-1}+\tfrac{1}{2}(p^2-p_0^2)^{1/2}R\,(p^2-p_0^2)^{1/2}\ . \quad (60)$$

Here $\bar{K}^J$ is the mutilated K^J matrix, where, as before[23], we cut out the $^3D_1$ ΣN waves, A^{-1} is the inverse scattering length matrix, R the effective range matrix, $p^{L+1/2}$ and $(p^2-p_0^2)^{1/2}$ are diagonal matrices with elements $p_i^{L+1/2}$ and $(p_i^2-p_0^2)^{1/2}$, where p_{0i} denotes the momentum at the $\Sigma^0 p$ threshold energy. In Table XIII we give the results for the effective range approximation.

The radius of convergence of ERA is 5 MeV, as determined by the pion-exchange cut. We did not find any poles within this region on the second Riemann sheet. We see that the situation in the soft-core model is quite different from, for example, model F, where we found poles at $E=2131.77\pm i2.39$ MeV on the second sheet, which again indicates that we now have a weaker interaction in the $^3S_1$ waves.

The ΛN P-wave scattering lengths and effective ranges are given in Table X. Comparing these values and the P-wave phase shifts in Table XI with those of the D and F models, it appears that these are qualitatively similar to those of model F and not model D. This seems favorable for $\Lambda-N$ well depths calculations.[43]

D. $\Sigma^- p$ scattering

1. $\Sigma^- p \to \Sigma^- p$

The fit to the total cross sections (for the precise definition see, e.g., Ref. 23) of the Heidelberg group[35] is given in Table VII and shown in Fig. 5. The data are well described ($\chi^2=2.6$ for six data points).

In Fig. 6 we compare the predicted angular distribution at $p_{\Sigma^-}=160$ MeV/c with the Heidelberg data (Ref. 35). The curve of the soft-core model for this distribution is intermediate to the ones obtained for models D and F.

In Table XIV we give the total nuclear cross sections for $\Sigma^- p$ elastic scattering up to $p_{\Sigma^-}=600$ MeV/c. Here

TABLE XIV. $\Sigma^- p \to \Sigma^- p, \Sigma^0 n, \Lambda n$ total cross sections in mb above the ΣN thresholds.

p_{Σ^-} (MeV/c)	T_{lab} (MeV)	$\Sigma^- p \to \Sigma^- p$	$\Sigma^- p \to \Sigma^0 n$	$\Sigma^- p \to \Lambda n$
50	1.0	547.9	575.1	757.3
100	4.2	176.5	207.6	254.4
150	9.4	138.1	116.7	136.1
200	16.6	123.6	74.9	87.5
250	25.8	108.6	51.1	62.2
300	37.0	91.0	37.2	47.1
350	50.1	74.0	29.0	37.3
400	65.0	59.7	23.9	30.4
450	81.8	48.7	20.3	25.3
500	100.2	40.4	17.5	21.5
550	120.3	33.9	15.3	18.5
600	141.9	29.1	13.5	16.1

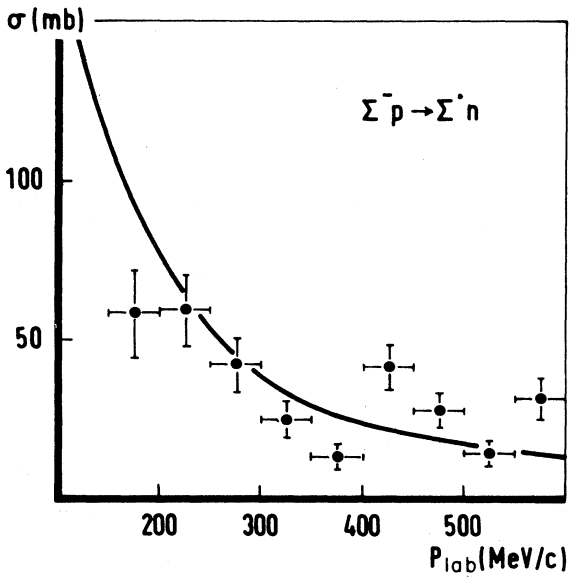

FIG. 8. Calculated $\Sigma^- p \to \Sigma^0 n$ total cross sections compared with the Massachusetts data (Ref. 37).

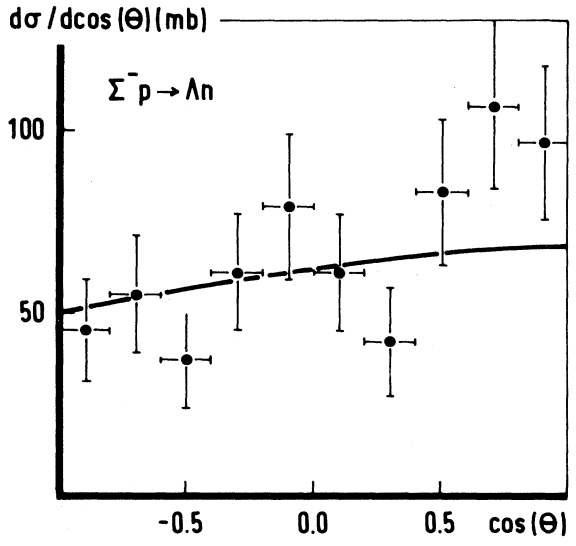

FIG. 10. Calculated $\Sigma^- p \to \Lambda n$ differential cross sections compared with experimental data (Ref. 32).

also as in D and F the scattering is mainly given by the $^3S_1$ wave for $p_{\Sigma^-} \leq 300$ MeV/c. At the higher energies the P waves dominate the total nuclear cross sections. The contributions of the higher L waves are always very small.

2. $\Sigma^- p \to \Sigma^0 n$

The calculated total cross sections are compared to the measurements of the Heidelberg group[32] in Table VII and Fig. 7. The result fits the data excellently, this of course with the exception of the datum at $p_{\Sigma^-} = 110$ MeV/c.

In Table XIV we give the total nuclear cross sections for $\Sigma^- p \to \Sigma^0 n$ up to $p_{\Sigma^-} = 600$ MeV/c. Here also as in D and F the scattering is dominated by the $^3S_1$ wave for $p_{\Sigma^-} \leq 250$ MeV/c. At the higher energies the P waves dominate the total nuclear cross sections. The contributions of the higher L waves are always very small. In Fig. 8 we compare the calculated total cross sections in the momentum region $150 \leq p_{\Sigma^-} \leq 600$ MeV/c with the unpublished data of the Massachusetts group (Ref. 37). In

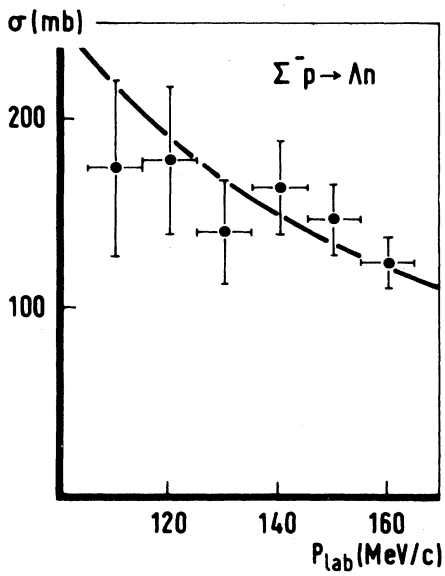

FIG. 9. Calculated $\Sigma^- p \to \Lambda n$ total cross sections compared with experimental data (Ref. 32).

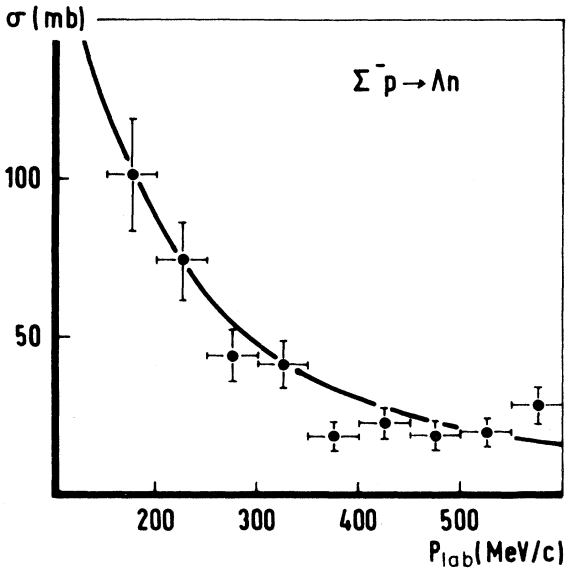

FIG. 11. Calculated $\Sigma^- p \to \Lambda n$ total cross sections compared with the experimental data of the Massachusetts group (Ref. 37).

contrast to the result of model D the soft-core model prediction agrees very well with these data.

3. $\Sigma^- p \to \Lambda n$

In Table VII and Fig. 9 we compare the calculated total cross sections with the measured values of the Heidelberg group (Ref. 32). A good fit is obtained which is comparable to that for model D and much better than for model F.

In Fig. 10 we compare the calculated angular distribution for $p_{\Sigma^-}=160$ Mev/c with the Heidelberg data (Ref. 32). The curve is rather flat, showing a rather small forward-backward ratio. This is as in model F, whereas the data tend to indicate a greater forward-backward ratio.

In Table XIV we give the total nuclear cross sections for $\Sigma^- p \to \Lambda n$ up to $p_{\Sigma^-}=600$ MeV/c. Below $p_{\Sigma^-}\simeq 200$ MeV/c is for 65% provided by the $^3S_1$-$^3S_1$ transition and for 25% by the $^3S_1$-$^3D_1$ transition. For $p_{\Sigma^-}\geq 350$ MeV/c these transitions account for 60% of the total cross sections. The other half is provided essentially by the P waves.

In Fig. 11 we compare the calculated total cross sections in the momentum region $150\leq p_{\Sigma^-}\leq 600$ MeV/c with the unpublished data of the Massachusetts group (Ref. 37). In contrast to the result of model D the soft-core model-prediction agrees rather well with these data.

Finally we mention the excellent value that we are able to reach for the inelastic capture ratio at rest $r_R=0.471$ (cf. Table VII) which is almost equal to the averaged experimental value.[15,36,37]

ACKNOWLEDGMENTS

We would like to thank Dr. B. Gibson and Dr. J. Carlson for their continued interest and useful comments. Also, we appreciate the encouragement from Prof. H. Bando. Finally, we thank Dr. E. Laenen and Dr. A. Verschuren for their help during the first stage of this work.

[1]M. M. Nagels, T. A. Rijken, and J. J. de Swart, Phys. Rev. D **17**, 768 (1978), referred to as (I). Note that in Eq. (15) of this reference there is an erroneous m^2 in front of ϕ_C^1.

[2]T. A. Rijken, in *Proceedings of the International Conference on Few Body Problems in Nuclear and Particle Physics, Quebec, 1974,* edited by R. J. Slobodrian, B. Cuec, and R. Ramavataram (Presses Université Laval, Quebec, 1975), p. 136; T. A. Rijken, Ph.D. thesis, University of Nijmegen, 1975.

[3]T. A. Rijken, Ann. Phys. (N.Y.) **164**, 1 (1985); **164**, 23 (1985).

[4]G. Veneziano, Nucl. Phys. **B117**, 519 (1976); E. Witten, *ibid.* **B160**, 57 (1979).

[5]M. M. Nagels, T. A. Rijken, and J. J. de Swart, Phys. Rev. D **12**, 744 (1975).

[6]M. M. Nagels, T. A. Rijken, and J. J. de Swart, Phys. Rev. D **15**, 2547 (1977).

[7]M. M. Nagels, T. A. Rijken, and J. J. de Swart, Phys. Rev. D **20**, 1633 (1979).

[8]F. E. Low, Phys. Rev. D **12**, 163 (1975); S. Nussinov, Phys. Rev. Lett. **34**, 1286 (1975).

[9]J. F. Gunion and D. E. Soper, Phys. Rev. D **15**, 2617 (1977); J. Pumplin and E. Lehman, Z. Phys. C **9**, 25 (1981).

[10]R. Dolen, D. Horn, and C. Schmid, Phys. Rev. **166**, 1768 (1968).

[11]H. Harari, Phys. Rev. Lett. **20**, 1395 (1968); F. J. Gilman, H. Harari, and Y. Zarmi, *ibid.* **21**, 323 (1968); H. Harari and Y. Zarmi, Phys. Rev. **187**, 2230 (1969).

[12]O. Dumbrajs *et al.*, Nucl. Phys. **B216**, 277 (1983).

[13]M. Nagels *et al.*, Nucl. Phys. **B147**, 189 (1979).

[14]B. Sakita and K. C. Wali, Phys. Rev. **139**, B1355 (1965).

[15]J. J. de Swart, M. M. Nagels, T. A. Rijken, and P. A. Verhoeven, Springer Tracts Mod. Phys. **60**, 138 (1971).

[16]R. H. Dalitz and F. von Hippel, Phys. Lett. **10**, 153 (1964).

[17]A. Gersten, P. A. Verhoeven, and J. J. de Swart, Nuovo Cimento **A26**, 375 (1975).

[18]A. A. Logunov and A. N. Tavkhelidze, Nuovo Cimento **29**, 380 (1963).

[19]R. Blankenbecler and R. Sugar, Phys. Rev. **142**, 1051 (1965).

[20]P. A. Verhoeven, Ph.D. thesis, University of Nijmegen, 1976.

[21]J. J. de Swart and C. K. Iddings, Phys. Rev. **128**, 2810 (1962).

[22]*Handbook of Mathematical Functions,* edited by M. Abramowitz and I. A. Stegun (Dover, New York, 1970).

[23]M. M. Nagels, T. A. Rijken, and J. J. de Swart, Ann. Phys. (N.Y.) **79**, 338 (1973).

[24]J. R. Bergervoet, P. C. van Campen, T. A. Rijken, and J. J. de Swart, Phys. Rev. Lett. **59**, 2255 (1987).

[25]Y. Yamamoto and H. Bando, Prog. Theor. Phys. Suppl. **81**, 9 (1985).

[26]R. L. Jaffe, Phys. Rev. D **15**, 267 (1977); **15**, 281 (1977).

[27]J. J. de Swart, T. A. Rijken, P. M. M. Maessen, R. G. E. Timmermans, and A. G. M. Verschuren, Proceedings of the 1986 International Symposium on Hypernuclear Physics, Tokyo, Japan, 1986 (unpublished).

[28]P. Povh and J. Hufner, Phys. Rev. Lett. **58**, 1612 (1987).

[29]H. Gomm, P. Jain, R. Johnson, and J. Schechter, Phys. Rev. D **33**, 801 (1986).

[30]H. Pilkuhn, Springer Tracts Mod. Phys. **55**, 168 (1970).

[31]C. B. Dover and A. Gal, in *Progress in Particle and Nuclear Physics,* edited by D. Wilkinson (Pergamon, New York, 1984), Vol. 12, p. 171.

[32]R. Engelmann, H. Filthuth, V. Hepp, and E. Kluge, Phys. Lett. **21**, 587 (1966).

[33]G. Alexander, U. Karshon, A. Shapira, G. Yekutieli, R. Engelmann, H. Filthuth, and W. Lughofer, Phys. Rev. **173**, 1452 (1968).

[34]B. Sechi-Zorn, B. Kehoe, J. Twitty, and R. A. Burnstein, Phys. Rev. **175**, 1735 (1968).

[35]F. Eisele, H. Filthuth, W. Fölisch, V. Hepp, E. Leitner, and G. Zech, Nucl. Phys. **B37**, 204 (1971).

[36]V. Hepp and M. Schleich, Z. Phys. **214**, 71 (1968).

[37]D. Stephen, Ph.D. thesis, University of Massachusetts, 1970.

[38]B. F. Gibson and D. R. Lehmann, Phys. Rev. C **10**, 888 (1974).
[39]J. A. Kadyk, G. Alexander, J. H. Chan, P. Gaposchkin, and G. H. Trilling, Nucl. Phys. **B27**, 13 (1971).
[40]J. M. Hauptman, J. A. Kadijk, and G. H. Trilling, Nucl. Phys. **B125**, 29 (1977).
[41]T. H. Tan, Phys. Rev. Lett. **79**, 338 (1973).
[42]O. Braun *et al.*, Nucl. Phys. **B124**, 45 (1977).
[43]J. Rozynek and J. Dabrowski, Phys. Rev. C **20**, 1612 (1979); J. Dabrowski and J. Rozynek, *ibid.* **23**, 1706 (1981).